Received: 01 April 2026 | Accepted: 23 July 2026 | Published online: 24 August 2026

DOI: 10.53550/ijsc.v54.i2.223

ORIGINAL ARTICLE

Indian Journal of Soil Conservation

Linking Visual Soil Erosion Indicators with FRN-^{137}Cs-Derived Soil Erosion Rates for Rapid Field-Based Soil Erosion Assessment in the Himalayan Region

Anu David Raj[1,2*] | **K.R. Sooryamol[3]** | **Suresh Kumar[4]** | **M. Sankar[3]**

[1]Agriculture and Soil Department, Indian Institute of Remote Sensing (IIRS), Indian Space Research Organisation (ISRO), Dehradun, India
[2]Forest Research Institute (FRI), Deemed to be University, Dehradun, India
[3]ICAR- Indian Institute of Soil and Water Conservation (IISWC), Dehradun, India
[4]Agriculture, Forestry and Ecology Group, Indian Institute of Remote Sensing (IIRS), Indian Space Research Organisation (ISRO), Dehradun, India

Corresponding Author:
E-mail: anudraj2@gmail.com

Handling Editor:
Dr. Brij Lal Lakaria

Key words:
Himalayas
Radioisotopes
Rapid field-based estimation
Soil loss
Visual soil erosion indicators

ABSTRACT

Soil erosion assessment in the Himalayan region is challenged by rugged terrain, intense rainfall, high spatial variability, and limited accessibility, making conventional monitoring methods expensive and difficult to implement. Although erosion models are widely applied, their accuracy is often constrained by the lack of field-based validation. Here, we developed and validated a practical framework that links visually observable soil erosion indicators with fallout radionuclide (FRN)-^{137}Cs-derived quantitative erosion rates to enable rapid field-based soil erosion assessment. A systematic field survey was conducted across the north-western Himalayas, where visual indicators of erosion, including sheet erosion, rills, gullies, pedestals, exposed roots, and surface coarse fragments were recorded at various sampling sites. Soil cores were simultaneously collected for ^{137}Cs analysis to quantify net soil erosion rates. Based on field observations, each site was assigned to a visual erosion class, which was subsequently compared with the corresponding ^{137}Cs-derived erosion class using Cohen's Kappa coefficient. The visual classification showed substantial agreement with the ^{137}Cs-derived erosion rates (Kappa = 0.72), demonstrating the reliability of the proposed approach. Classification accuracy was highest for the extreme erosion classes (85–86%), whereas the intermediate classes exhibited lower agreement (66–69%), reflecting the inherent difficulty in distinguishing transitional erosion stages under field conditions. Soil physicochemical properties further validated the classification, with soil organic carbon declining and bulk density increasing consistently with erosion severity. Forest and grassland soils maintained higher organic carbon and better structural condition, whereas barren lands exhibited depleted carbon stocks, greater compaction, and more degraded soil quality. The resulting visual indicator-erosion rate framework provides a rapid, low-cost, and instrument-free approach for estimating soil erosion severity in mountainous landscapes. As the framework relies only on observable field indicators and validated reference tables, it can be readily applied by researchers, land managers, and policymakers for erosion mapping, field validation of erosion models, and the development of machine-learning-based erosion prediction models in data-scarce environments.

1 | INTRODUCTION

Soil erosion is one of the most pervasive forms of land degradation, with profound implications for soil fertility, ecosystem stability, carbon cycling, climate change, and downstream sediment dynamics (David Raj *et al*., 2024a). Mountain ecosystems are particularly vulnerable because of their steep terrain and dynamic geomorphic processes, and among these, the Himalayas represent one of the most erosion-prone regions globally. Their steep and highly dissected topography, fragile lithology, active tectonics, and climate change-induced intensification of monsoonal rainfall collectively accelerate soil detachment and transport (David Raj *et al*., 2022; Gupta and Kumar, 2017). These natural factors, combined with increasing anthropogenic disturbances such as deforestation and unsustainable land-use change, have substantially increased erosion susceptibility across the region. Consequently, soil erosion in the Himalayas exhibits high spatial heterogeneity and temporal variability, posing significant challenges for its accurate quantification and effective management (Singh *et al*., 2019; Sooryamol *et al*., 2022).

Despite its environmental significance, reliable estimation of soil erosion in mountainous landscapes remains challenging (Borrelli *et al.*, 2021; Kumar *et al.*, 2024a). Direct field-based measurements are often constrained by difficult accessibility, rugged terrain, and harsh climatic conditions, limiting long-term monitoring and dense spatial sampling (Kumar *et al.,* 2024a). Consequently, most erosion assessments rely on empirical or conceptual models such as the Revised Universal Soil Loss Equation (RUSLE), Universal Soil Loss Equation (USLE), and Morgan–Morgan–Finney (MMF) model (Chandrakala *et al*., 2024; Jain *et al*., 2001; Joshi *et al*., 2023; Kalambukattu *et al*., 2021; Uppengal *et al*., 2026). Although these models provide valuable information on erosion patterns and relative erosion risk, their performance depends heavily on input parameterization and field validation. In complex mountainous terrain, where parameter uncertainty is inherently high, the limited availability of independent field observations introduces considerable uncertainty into erosion estimates and reduces their reliability for site-specific conservation planning (Batista *et al*., 2019).

Among the available field-based techniques, fallout radionuclides (FRNs), particularly Caesium-137 (^{137}Cs), have emerged as robust tracers for quantifying long-term soil redistribution (David Raj *et al.*, 2025a; David Raj *et al*., 2024b; Mariappan *et al*., 2022). The ^{137}Cs technique integrates erosion and deposition processes over decadal timescales and provides spatially distributed estimates that are less affected by short-term climatic variability. However, despite their scientific robustness, FRN techniques require specialized laboratory facilities, skilled personnel, and carefully designed sampling strategies, making them resource-intensive and limiting their routine application for operational soil erosion assessment (IAEA, 2014; Mabit *et al.*, 2018).

An alternative approach is the use of visual soil erosion indicators, including sheet erosion, rills, gullies, pedestals, exposed roots, surface sealing, and presence of coarse fragments. These indicators represent direct field evidence of ongoing or past erosion processes and are widely used in rapid field assessments because they are inexpensive, easy to identify, and require no specialized equipment (Okoba and Sterk, 2006a,b; Salhi *et al.*, 2023). Moreover, they integrate the cumulative effects of erosion at a given location, making them suitable for practical field applications. However, visual indicators remain largely qualitative and subjective, relying heavily on observer experience. More importantly, there is currently no standardized framework that quantitatively relates these observable indicators to actual soil erosion rates. Without quantitative calibration, visual observations cannot be reliably used for model validation, comparison of erosion severity among sites, or evidence-based land management decisions. This limitation is particularly important in the Himalayas, where logistical constraints and data scarcity necessitate simple, rapid, and scalable field assessment methods. Previous work by Okoba and Sterk (2006a) proposed a visual indicator-based framework for assessing soil erosion; however, their methodology relied primarily on plot-scale measurements of rills and lacked independent quantitative validation. To date, no study has systematically calibrated multiple visual soil erosion indicators against independently measured soil erosion rates using fallout radionuclides under the complex environmental conditions of the Himalayan region.

HIGHLIGHTS

- Visual soil erosion indicators validated with ^{137}Cs-derived soil erosion rates.
- Rapid, low-cost field method for erosion assessment in Himalayas.
- Strong agreement (Kappa = 0.72) validates visual classification.
- Soil quality declines consistently with increasing erosion severity.
- Scalable tool for model validation and ML-based erosion mapping.

To address this gap, the present study develops and validates an integrated framework linking visual soil erosion indicators with ^{137}Cs-derived soil erosion rates. Visual indicators were systematically documented across diverse land-use types and topographic settings and calibrated against independently measured radionuclide-derived erosion rates. Agreement between visually interpreted erosion classes and quantitative erosion estimates was evaluated using Cohen's Kappa statistic, enabling the development of a validated visual indicator–erosion rate reference framework. Unlike previous approaches, the proposed framework establishes quantitative erosion-rate ranges associated with easily identifiable field indicators, allowing erosion severity to be estimated rapidly without specialized instrumentation.

The developed framework has considerable practical significance for both research and land management. It provides a rapid, low-cost, and instrument-free method for assessing soil erosion in inaccessible mountainous environments, enabling field practitioners to estimate erosion severity using observable indicators and calibrated reference tables. In addition to facilitating rapid field assessment, the framework offers an independent means of validating soil erosion models and provides reliable training data for emerging machine-learning applications. By bridging the gap between rigorous radionuclide-based measurements and practical field observations, this study advances an operational and scalable approach for soil erosion assessment, supporting researchers, watershed managers, policymakers, and local stakeholders in developing evidence-based soil and water conservation strategies, particularly in data-scarce mountain regions such as the Himalayas.

2 | Study Area

A representative catchment of the north-western Himalayas was selected for the present study. The Tehri Dam catchment, located on the Bhagirathi River approximately 145 km downstream of the Gangotri Glacier, covers an area of about 7,293 km². Geographically, it extends from 78°9′15″ E to 79°24′55″ E longitude and 30°20′20″ N to 31°27′30″ N latitude, with elevations ranging from nearly 600 m at the dam site to about 7,000 m in the upper glaciated regions (Fig. 1). The climate of the region is classified as Cwb and Dwb according to the Köppen classification (Beck *et al.*, 2018), reflecting temperate to cold conditions with strong altitudinal variability. Annual precipitation ranges from 1,016 mm to 2,630 mm (IMD gridded data; Pai *et al*., 2014). The mean maximum and minimum temperatures are 29.4°C and 14.7°C in Tehri-Garhwal, and 23.6°C and 13.1°C in Uttarkashi, respectively (IMD, 2014). Geologically, the catchment encompasses three major litho-tectonic units: the Lesser, Higher, and Trans-Himalayan zones. The Lesser Himalayas include the Jaunsar and Garhwal groups, dominated by phyllite, quartzite, limestone, and shale. The Higher Himalayas are characterized by the Central Crystalline complex comprising gneiss, mica schist, garnet, and granite. The Trans-Himalayan region includes formations such as the Sumna group and Bhilangana River units, consisting of granite gneiss, argillite, limestone, and quartzite (Chauhan *et al.*, 2022). Soils in the catchment show considerable variability with elevation and terrain. High-altitude slopes are dominated by shallow, well-drained, sandy-skeletal Lithic Cryorthents, whereas hill forests are characterized by loamy Udorthents and Eutrochepts. Soils in the Lesser Himalayas are typically loamy-skeletal, moderately acidic, and rich in organic carbon, while fluvial valleys contain Udifluvents and Eutrochepts with moderate to high organic content and slightly alkaline pH (Sidhu and Surya, 2014). Land use in the catchment is heterogeneous, comprising forests, grasslands, agricultural lands, scrublands, barren areas, and settlements. The dominant vegetation includes chir pine (*Pinus roxburghii*), banj oak (*Quercus leucotrichophora*), deodar (*Cedrus deodara*), and buransh (*Rhododendron arboreum*). Agricultural practices are seasonal, with rice, maize, and finger millet cultivated during the kharif season, and wheat and barley grown during the rabi season (KVK, n.d.).

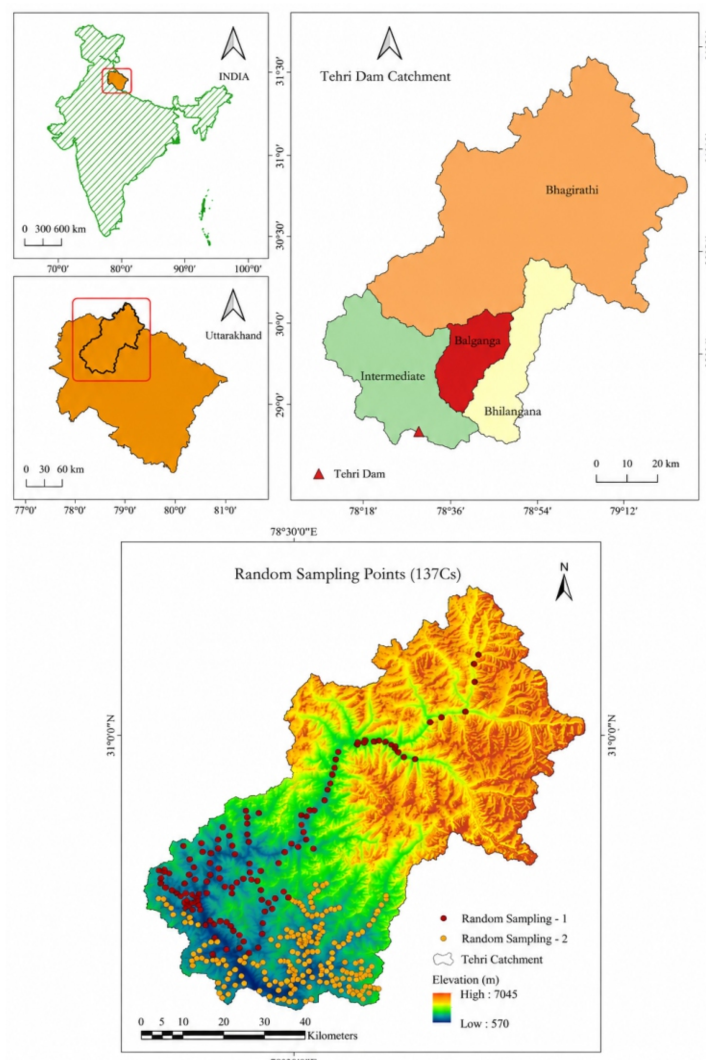

FIGURE 1 Location of the study area.

3 | MATERIALS AND METHODS

The methodological framework of the study is presented in Fig. 2.

3.1 | Soil Sampling Strategy

A ^{137}Cs-based approach was employed to measure soil erosion across the study area, using data derived from the thesis of Raj (2025) and published literatures (David Raj *et al.*, 2025 a & b; David Raj *et al.*, 2024 b, c, d & David Raj *et al.*, 2026; Kumar *et al.*, 2024b). Establishing a reliable reference inventory is a critical prerequisite in FRN-^{137}Cs based studies. Accordingly, undisturbed reference sites were selected based on standard criteria, including long-term stability since the 1950s, absence of erosion or deposition processes, and relatively flat terrain under permanent vegetation cover (e.g., grassland). Soil samples were collected using stainless steel sampling devices from soil profiles extending up to the depth of ^{137}Cs penetration or until parent material was encountered (David Raj and Kumar, 2024). Sampling was conducted at regular depth intervals with multiple replications to minimize uncertainty, following established protocols (Loughran *et al.*, 2002; Mariappan *et al.*, 2022).

Given the logistical constraints of mountainous terrain, measured reference inventories were supplemented with modelled global fallout estimates of Caesium-137 tracing, incorporating rainfall-based corrections. Spatial interpolation of reference inventories was performed using the Thiessen polygon method, assuming relatively uniform fallout distribution within defined zones. For catchment-scale sampling, a stratified sampling framework was developed using soil-landscape units derived from topographic position (via Topographic Position Index) and land use/land cover data. This approach accounts for variability in erosion processes driven primarily by slope position and land use in mountainous regions (Kumar *et al.*, 2023). Representative sites from each land-use unit were selected using a stratified random sampling design. Soil cores were collected using cylindrical corers to depths appropriate for the prevailing land-use and site conditions. For ^{137}Cs measurements, soil cores were collected to the full depth of ^{137}Cs penetration, which varied from 35 to 60 cm depending on local conditions. In total, 371 plot samples were collected and analysed for soil erosion assessment.

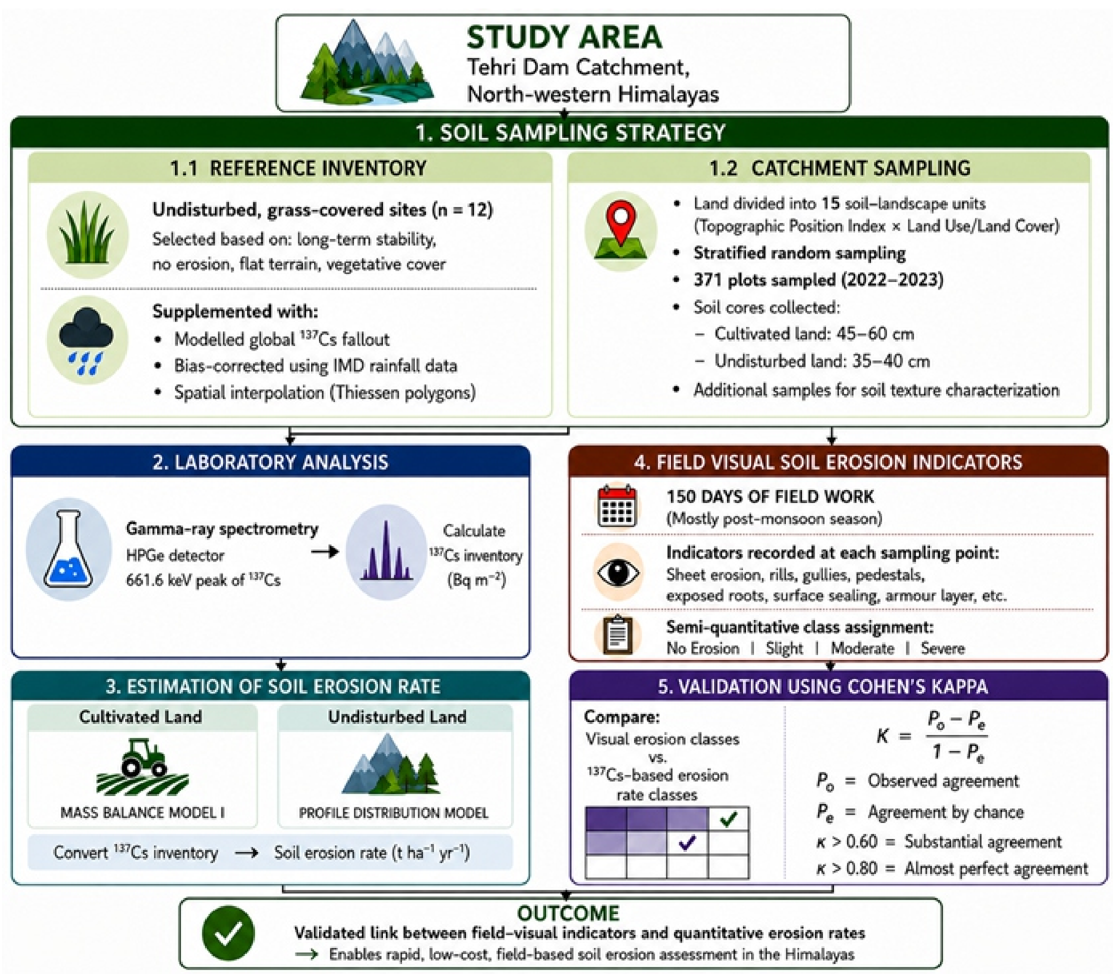

FIGURE 2 Methodology flowchart of the study.

3.2 | Physico-chemical analysis of soils

Surface soil samples (0-15 cm) were collected and analysed for key physicochemical properties, including soil texture, bulk density, pH, electrical conductivity (EC), and organic carbon, following standard laboratory procedures. A total of 556 independent soil samples were collected from the 0-15 cm surface layer across the study area for physicochemical characterization. All analyses were conducted at the Central Analytical Laboratory (CAL), Indian Institute of Remote Sensing (IIRS), Dehradun, following established protocols.

3.3 | Estimation of soil erosion rates

The activity concentration of ^{137}Cs in soil samples was determined using gamma spectrometry with a high-purity germanium (HPGe) detector (BEGE 5030, Canberra Industries Inc., USA), having 48% relative efficiency. Each sample (250-350 g) was counted for 60,000 seconds, and ^{137}Cs activity was quantified from the 661.6 keV gamma peak. The detector system, available at the Centre for Advanced Research in Environmental Radioactivity (CARER), Mangalore University, was calibrated following established protocols, as detailed in previous studies (Karunakara *et al*., 2013; Mohan *et al*., 2019). The total ^{137}Cs inventory (Bq m^{-2}) at each sampling location was calculated from measured activity concentrations, soil bulk density, and sampling depth.

Soil erosion and deposition rates were subsequently estimated from the measured ^{137}Cs inventories using established conversion models. The Mass Balance Model I was applied to cultivated (ploughed) agricultural sites, whereas the Profile Distribution Model was used for undisturbed sites, including forest, grassland, scrubland, and barren land (Walling *et al*., 2007). In cases where depth-wise ^{137}Cs activity profiles were available, the Modelling Deposition and Erosion rates with RadioNuclides (MODERN) model was also employed (Arata *et al*., 2016), following approaches adopted in previous studies. These models estimate long-term soil redistribution rates by relating deviations in ^{137}Cs inventories from the reference inventory to net soil loss or deposition.

3.3.1 | Mass balance model-I

$$Y = \frac{10dB}{P}\left[1-\left(1-\frac{X}{100}\right)^{\frac{1}{t-1963}}\right]$$

Y = mean annual soil loss (t ha^{-1} year^{-1}); d = depth of plough or cultivation layer (m); B = bulk density of soil (kg m^{-3}); X = percentage reduction in total ^{137}Cs inventory P = particle size correction factor.

3.3.2 | Profile distribution model

$$Y = \frac{10}{(t-1963)P} ln\left(1-\frac{X}{100}\right)h_o$$

Y = annual soil loss (t ha^{-1} year^{-1}); t = year of sample collection (yr); X = percentage ^{137}Cs loss in total inventory in respect to the local ^{137}Cs reference value; h_0 profile shape factor of (kg m^{-2}) and (P=1) particle size correction factor was used.

3.4 | Observation of visual soil erosion indicators

Visual soil erosion indicators were systematically recorded at each ^{137}Cs sampling location through detailed field observations. A total of 150 field days were spent surveying the study area to ensure adequate spatial coverage across different land-use types and topographic conditions. Field surveys were conducted primarily during the post-monsoon season, when erosion features are most distinct following peak rainfall events. The presence, extent, and severity of key visual erosion indicators, including sheet erosion (surface soil removal and colour change), rills, gullies, pedestals, exposed roots, surface sealing, and surface coarse fragments, were documented following standardized field protocols. At each sampling location, all visible erosion features were assessed, and multiple indicators, when present, were collectively evaluated to characterize the overall erosion condition.

A semi-quantitative classification scheme was used to minimize observer subjectivity. Based on the intensity and spatial expression of the observed indicators, each site was assigned to one of seven erosion severity classes: E0 (no erosion), E1 (very slight erosion; 0-5 t ha^{-1} yr^{-1}), E2 (slight erosion; 5-10 t ha^{-1} yr^{-1}), E3 (moderate erosion; 10-15 t ha^{-1} yr^{-1}, E4 (moderately severe erosion; 15-20 t ha^{-1} yr^{-1}), E5 (severe erosion; 20-40 t ha^{-1} yr^{-1}), and E6 (very severe erosion; >40 t ha^{-1} yr^{-1}). The visually assigned erosion classes were subsequently compared with the corresponding ^{137}Cs-derived soil erosion rates to evaluate the relationship between qualitative field observations and quantitative soil erosion measurements. This comparison formed the basis for training the visual indicator–erosion rate framework developed in this study.

3.5 | Validation of visual indicators with soil erosion rates

The reliability of field-based visual soil erosion indicators was evaluated by comparing the observed erosion classes with quantitative soil erosion rates derived from ^{137}Cs analysis. Both datasets were classified into comparable erosion severity classes (E0-E6), enabling direct class-to-class comparison. To ensure independent and robust validation, the complete dataset (n = 371) was divided into a training dataset (80%, n = 297) and a validation dataset (20%, n = 74) using stratified random sampling while preserving class proportions. The training dataset was used to establish the classification framework, whereas the validation dataset was used exclusively for independent accuracy assessment.

The level of agreement between the visual classification and the ^{137}Cs-based erosion estimates was assessed using Cohen's Kappa coefficient (κ), which accounts for agreement occurring by chance. The Kappa coefficient is expressed as:

$$\kappa = \frac{P_o - P_e}{1 - P_e}$$

Where, (P_o) is the observed agreement (proportion of correctly classified samples), (P_e) is the expected agreement by chance, calculated from the marginal totals of the confusion matrix.

The expected agreement is given by:

$$P_e = \sum \frac{(R_i \, X \, C_i)}{N^2}$$

Where Ri and Ci are the row and column totals for class i, and N is the total number of samples.

The value of κ ranges from -1 to 1, where values closer to 1 indicate strong agreement, values around 0 indicate agreement no better than random chance, and negative values indicate disagreement. In general, κ values > 0.60 are considered to represent substantial agreement, while values > 0.80 indicate almost perfect agreement. The use of an independent validation dataset, combined with confusion matrix-based accuracy metrics, provides a robust statistical framework for evaluating the effectiveness of visual indicators in representing actual soil erosion severity. This approach ensures that the classification framework is not only internally consistent but also generalizable, supporting its application as a reliable and cost-effective field-based assessment tool.

4 | RESULTS AND DISCUSSION

4.1 | Physico-chemical characterization of soils

4.1.1 | Soil pH

Soil pH across the study area ranged from strongly acidic to slightly alkaline (3.1-8.2), with a mean value of 5.5 ± 0.9, indicating predominantly moderately acidic conditions (Fig. 3). Grassland soils exhibited significantly lower pH (4.7 ± 0.6) compared to other land use/land cover (LULC) types ($P < 0.05$), whereas forest (5.4 ± 1.0), agricultural (5.5 ± 0.8), and scrubland soils (5.6 ± 0.9) showed no significant differences. Soil acidification in forest and grassland ecosystems is primarily driven by carbonic acid formation from CO_2 released during root respiration and microbial activity, along with contributions from organic acids and atmospheric deposition (Müller *et al.*, 2022). Slightly higher pH values in agricultural soils may be attributed to management practices aimed at maintaining soil fertility.

4.1.2 | Soil electrical conductivity (EC)

The soils were non-saline, with EC values ranging from 2 to 844 µS cm^{-1} (mean: 93.7 ± 112.9 µS cm^{-1}), indicating high spatial variability (Fig. 3). Grassland soils showed significantly higher EC (188.1 ± 160.6 µS cm^{-1}) compared to other LULC types ($P < 0.05$), while forest (89.3 ± 98.6 µS cm^{-1}), agricultural (88.9 ± 113.8 µS cm^{-1}), and scrubland soils (100.8 ± 118.7 µS cm^{-1}) did not differ significantly. Higher EC in grasslands may be linked to the presence of calcium-rich parent material (limestone), whereas lower EC in cultivated soils is likely due to leaching and erosion of soluble bases under continuous agricultural practices (Jaleta Negasa, 2020). These findings are consistent with previous studies reporting relatively higher EC in natural ecosystems compared to cultivated lands.

4.1.3 | Soil texture and composition

According to USDA classification, soils were predominantly loamy, with sandy loam (45%) and loam (38%) as the dominant textural classes, followed by silt loam and other minor classes (Fig. 3 and 4). Sand content was highest in scrubland (60.9 ± 12.1%), followed by forest (55.6 ± 10.9%), agriculture (47.9 ± 13.9%), and grassland (40.0 ± 15.3%), with significant differences across all LULC types ($P < 0.05$). Silt content was comparatively higher in agricultural soils (33.6 ± 11.6%), likely due to terrace farming, which traps fine sediments from upslope areas. Terrace farming is primarily adopted in the agriculture land which effectively traps fine sediments from the upslope area (Mekonnen *et al.*, 2015) and results in higher silt content than the forest soils. Clay content was highest in grasslands (31.4 ± 22.4%), reflecting reduced erosion and better retention of fine particles under dense vegetation cover. The presence of vegetation minimizes selective removal of fine fractions, thereby maintaining higher silt and clay content (Koiter *et al.*, 2017). Overall, texture variations highlight the influence of both erosion processes and land management practices, with coarser fractions dominating in degraded landscapes and finer particles retained in stable, vegetated areas.

4.1.4 | Soil bulk density (BD)

Bulk density ranged from 0.61 to 1.53 g cm^{-3}, with a mean of 0.97 ± 0.16 g cm^{-3} (Fig. 3). The highest BD was observed in scrubland (1.21 ± 0.11 g cm^{-3}), followed by agriculture (0.97 ± 0.13 g cm^{-3}) and grassland (0.92 ± 0.20 g cm^{-3}), while forest soils exhibited the lowest values (0.91 ± 0.16 g cm^{-3}). Significant differences were observed among most LULC types ($P < 0.05$). Lower BD in forest soils is associated with higher organic matter content, bioturbation, and improved soil structure, whereas higher BD in scrubland reflects reduced organic inputs and soil compaction (Meusburger *et al.*, 2013). The inverse relationship between bulk density and soil organic carbon is well established (Dexter *et al.*, 2005; Keller and Håkansson, 2010).

4.1.5 | Total soil organic carbon (SOC)

The total organic carbon (TOC) content in the soils ranged from 0.3 to 22.7% with a mean value of 3.3 ± 2.3 % (Fig. 4). The high TOC was found in the grassland soils (8.3 ± 6 %), followed by forest (3.9 ± 2.5 %), scrubland (2.8 ± 1.9 %) and agriculture (2.7 ± 1.3 %). Except agriculture and scrubland all other land use/land cover combinations were statistically different at a P value of <0.05. Yang *et al.* (2018) reported SOC concentrations of 7.61 ± 0.53% in the upper 10 cm of a

Peruvian alpine grassland and 10.54 ± 0.07% in the upper 20 cm of Venezuelan Andean grassland soils (Sarmiento and Bottner, 2002). In general, high soil organic carbon content can be found in grassland as well as forest soils (Padarian *et al*., 2022). Dorji *et al*., (2014) found that forest and grass land soils has high soil organic carbon compared to cultivated regions. Nadelhoffer *et al*., (2004) stated that plant litter and root influences the soil organic matter production. Excessive tillage and intensive cultivation can reduce soil organic carbon from the agricultural soils (Singh *et al*., 2007). In scrubland due to the absence of sufficient cover selectively removed the fine particle this eroded soil experiences a significant reduction in its soil organic matter pool (Óskarsson *et al*., 2004). This pattern of TOC variation across different land uses and land cover types aligns well with the distribution of bulk density observed in the Tehri Dam catchment area.

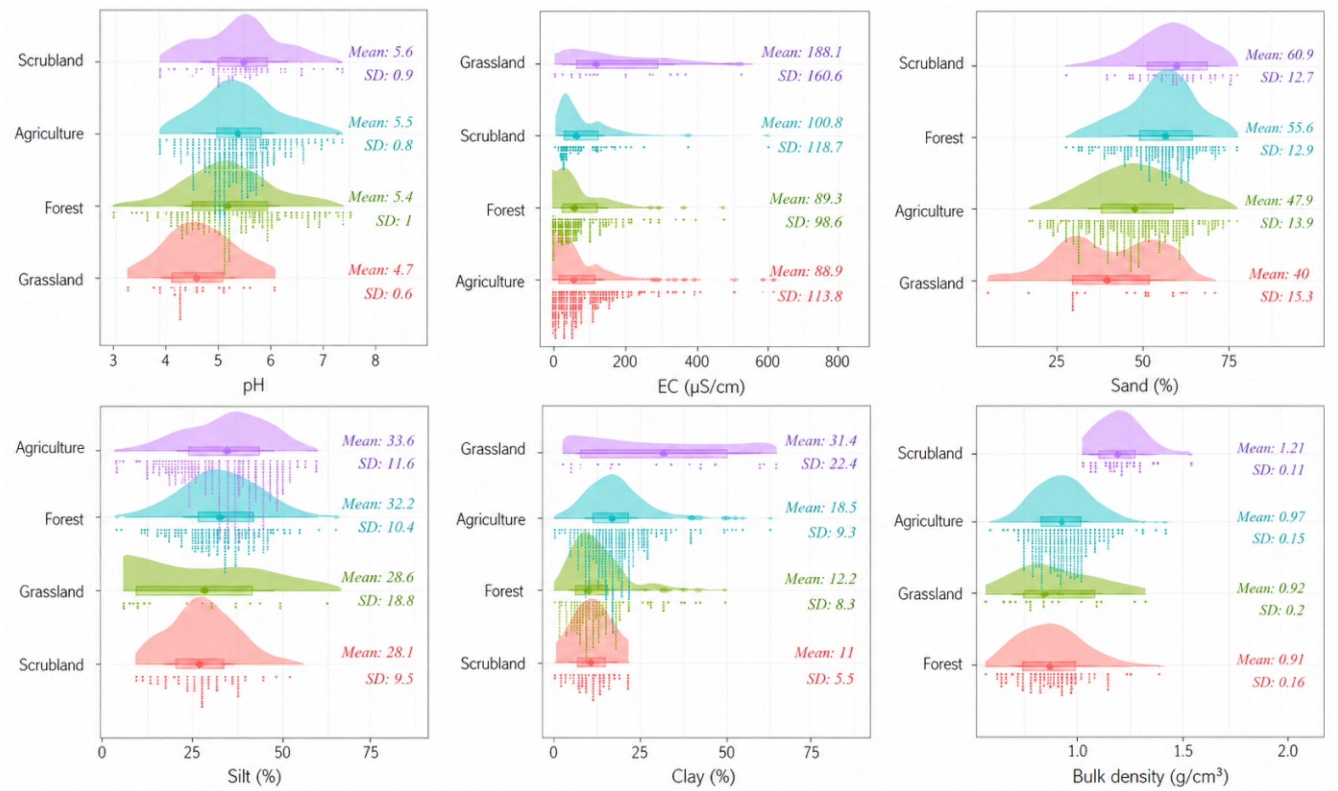

FIGURE 3 Distribution of soil pH, EC, textural composition and soil bulk density using rain-cloud plot.

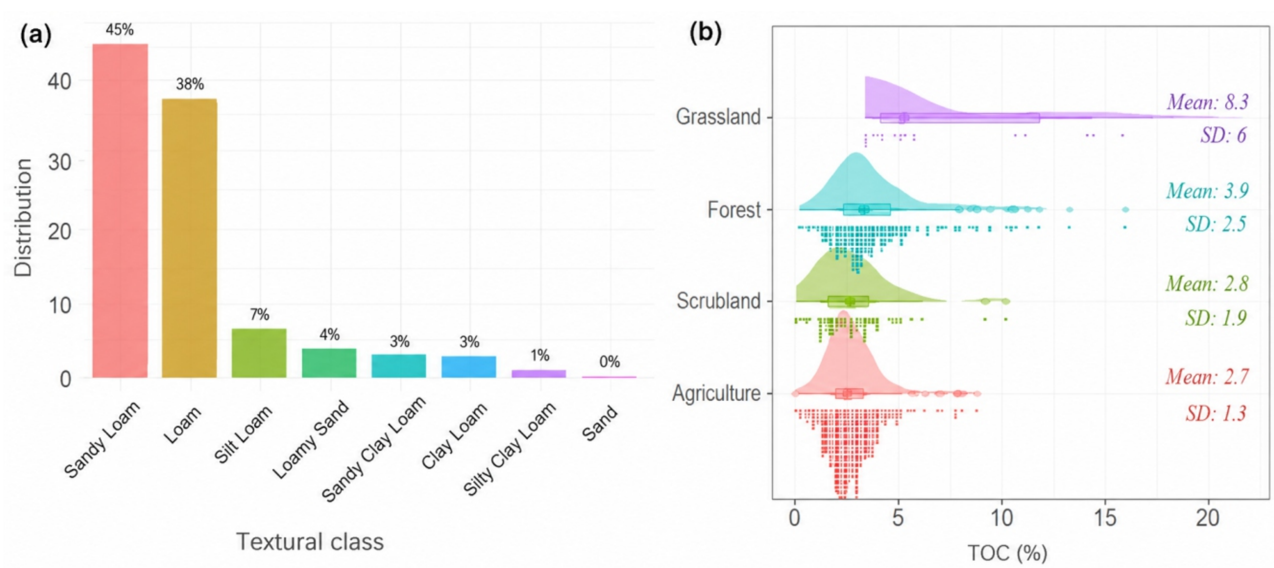

FIGURE 4 Distribution of (a) soil textural classes and (b) soil organic carbon in the study area.

4.2 | Field survey-based characterization of soil erosion process

Understanding the dynamics of soil erosion in the Himalayan environment is inherently challenging due to pronounced spatial and temporal variability in landscape characteristics. The nature and intensity of erosion processes vary with observation scale, season, and prevailing environmental conditions, which strongly influence their perception and interpretation. To capture this variability, extensive field surveys were conducted primarily during the post-monsoon (September-November) and pre-monsoon (March-June) periods, thereby avoiding the peak rainfall and snowfall seasons that restrict accessibility and obscure surface indicators. These observation windows allowed clearer identification of erosion features formed during the monsoon while minimizing interference from active precipitation events.

Field observations indicate that soil erosion processes in the Himalayan region are highly dynamic and often transient, driven by the interplay of steep slopes, fragile lithology, and high-intensity rainfall. Many erosion features, particularly those associated with surface runoff, are short-lived and may be rapidly modified or obliterated by subsequent events. Nevertheless, several distinct and recurring indicators of erosion were systematically identified across the study area, providing valuable insights into the dominant erosion processes and their spatial distribution. These field-based observations form a critical basis for linking qualitative visual indicators with quantitative soil redistribution rates derived from FRN-^{137}Cs measurements, thereby enabling a more robust and rapid assessment of soil erosion in complex mountainous terrains.

4.2.1 | Reconnaissance observations in the catchment

Representative field photographs of the observed erosion features are presented in Fig. 5. The reconnaissance survey across the Himalayan catchments revealed a wide spectrum of erosion processes, varying in form, persistence, and spatial dominance. Splash, sheet, and rill erosion were commonly observed but were generally short-lived due to rapid surface modification under high-intensity rainfall and steep slopes. Splash erosion was particularly evident in areas with sparse or absent vegetation cover and soils of low structural resistance, where raindrop impact initiates particle detachment. These early-stage erosion processes play a crucial role in weakening soil structure and enhancing susceptibility to further detachment and transport. In particular, cultivated and recently ploughed soils were found to be more prone to crust formation and sheet erosion (Legout *et al*., 2005). In contrast, gully erosion emerged as the most prominent and persistent form of land degradation across the study area. Gullies were often deep and elongated, frequently evolving into first-order drainage channels. Their occurrence was widespread in scrublands, sparsely vegetated areas, and even within forested regions. In forested terrains, topographic controls facilitate the concentration of overland flow into natural depressions, accelerating incision and gully expansion. Although terracing in cultivated lands disrupts slope continuity and reduces flow velocity, localized concentration of runoff between terraces, particularly on steep and highly dissected slopes, can still initiate gully formation. Significant variations in drainage characteristics were observed among the sub-catchments. The Bhagirathi sub-catchment exhibited a well-developed, deeply incised, and extensive drainage network, whereas the Bhilangana and Balganga catchments showed relatively smaller and less complex systems. The Balganga catchment, characterized by dense forest cover, displayed comparatively lower drainage density. Consistent with previous studies (Clubb *et al.*, 2016), areas with higher drainage density were associated with increased erosion intensity, reflecting more efficient runoff conveyance and sediment transport.

Riverbank erosion was a pervasive feature throughout the drainage network. The steep gradients typical of Himalayan rivers enhance flow velocity, increasing their erosive power. Moreover, during high-flow conditions, rivers often exceed their sediment transport capacity, leading to bank undercutting and channel widening. Such processes are further intensified during extreme hydrological events, including cloudbursts, intense convective storms, and glacial lake outburst floods (GLOFs), which significantly amplify runoff and sediment flux within the catchments. Overall, these reconnaissance observations highlight the complex interplay of topography, land cover, and hydrological dynamics in governing soil erosion processes in the Himalayan region, providing a vital field-based context for interpreting FRN-^{137}Cs-derived soil redistribution patterns.

4.2.2 | Topographic controls on soil erosion

Topographic aspect exerts a significant control on vegetation distribution, soil moisture conditions, and consequently, soil erosion processes across the Himalayan catchments. A clear contrast was observed between northern and southern slope aspects in all sub-catchments. The northern aspects are predominantly covered with dense natural vegetation, supported by relatively lower solar insolation, cooler microclimatic conditions, and higher soil moisture retention. These conditions favour the growth of species such as Rhododendron, Deodar, and Oak (Fig. 6a). In contrast, the southern aspects receive higher solar radiation, resulting in warmer and relatively drier conditions that are more suitable for agricultural activities. As a result, these slopes are largely converted into cultivated lands and are often interspersed with Pine-dominated forests. Field observations indicate that vegetation cover on southern aspects is comparatively sparse, reducing surface protection against raindrop impact and overland flow Consequently, these slopes are more susceptible to soil erosion (del Pino and Ruiz-Gallardo, 2015). The southern aspects also exhibit a more dissected terrain, characterized by the presence of exposed bedrock, permanent gullies, and enhanced surface runoff pathways (Fig. 6b). In several cultivated areas, this dissection is further accentuated by improper land management and slope modification. Geologically, the catchment primarily representing the Lesser and Middle Himalayas are dominated by sedimentary formations with relatively low structural strength. These weak lithological units are highly vulnerable to erosion and facilitate rapid soil detachment and transport. Moreover, such conditions increase the susceptibility of these areas to mass wasting processes, including landslides, particularly under intense rainfall events (Fig. 6a). Overall, the combined influence of aspect-driven microclimate, vegetation cover, and lithological characteristics plays a critical role in governing the spatial variability of soil erosion across the Himalayan landscape.

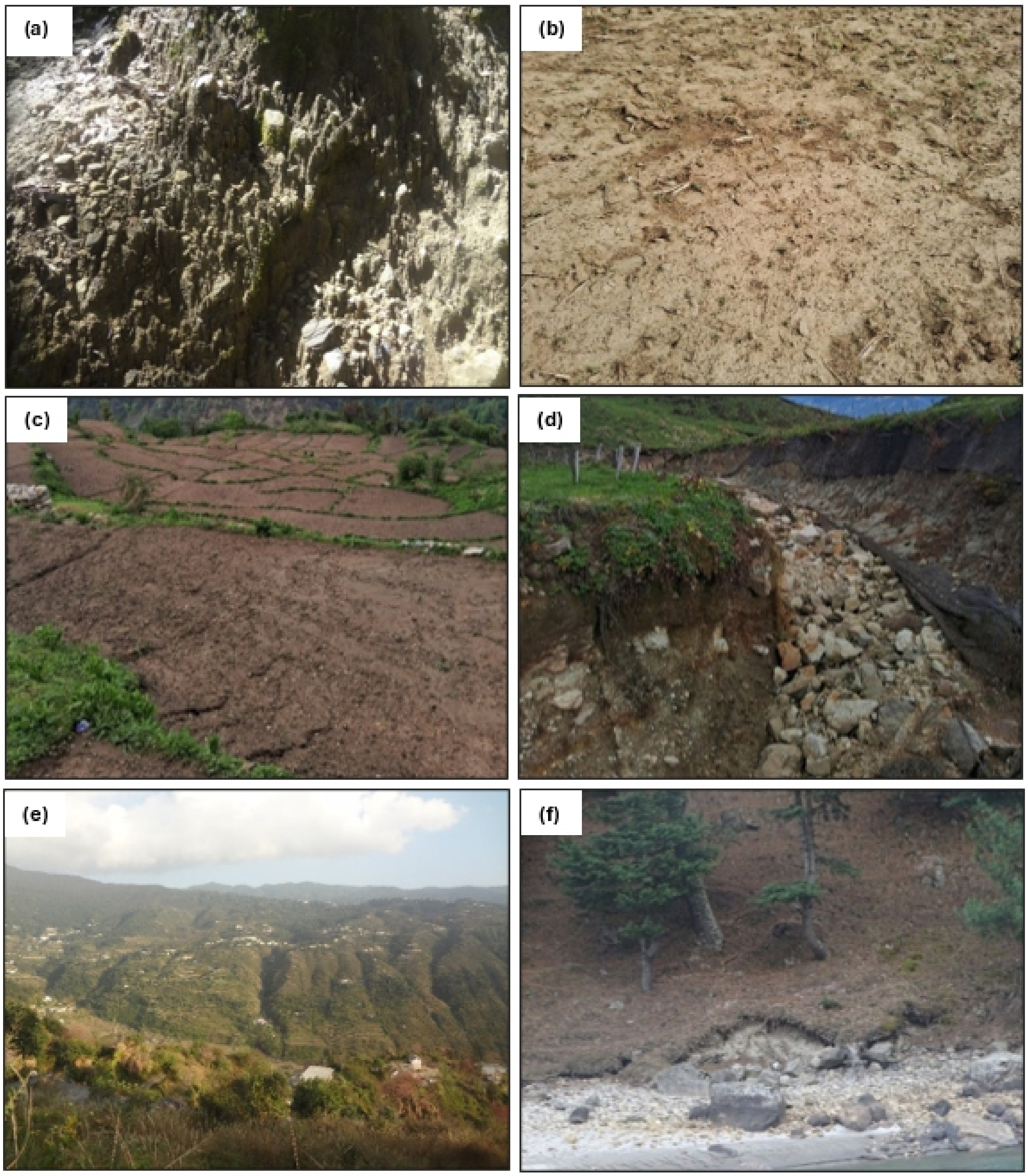

FIGURE 5 Different types of soil erosion observed in the Tehri dam catchment (a) splash erosion - visible removal of soil particles by raindrop impact, (b) sheet erosion - a thin layer of topsoil removed uniformly across the surface, (c) rill erosion - small, narrow channels formed by concentrated water flow, (d) advancing gully - deeply incised channels formed by progressively concentrated water flow, (e) well-developed gully - under high rainfall and steep slope conditions, and (f) riverbank erosion - scouring and undercutting of riverbanks by flowing water.

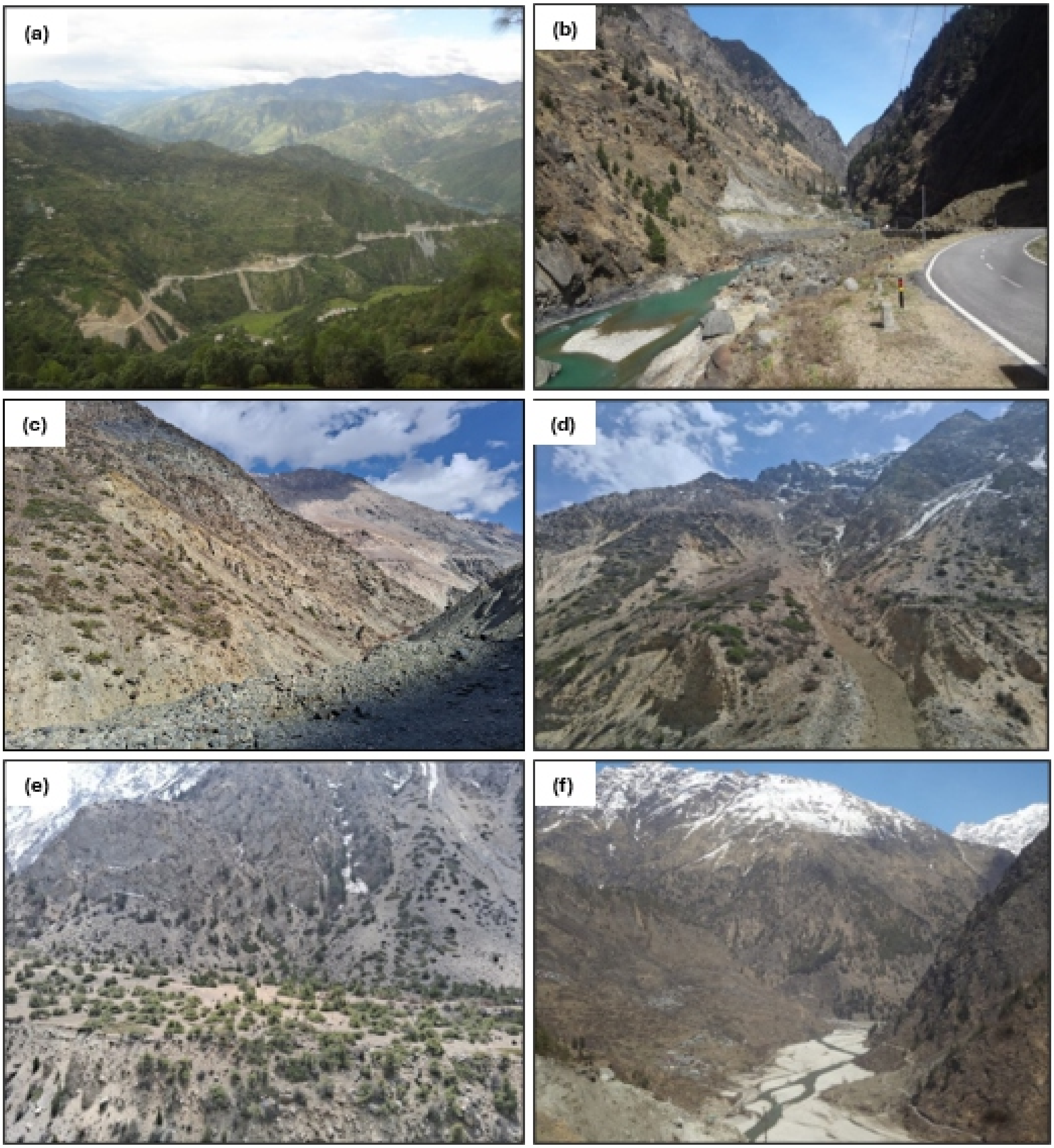

FIGURE 6 (a) High landslide-prone middle Himalayas (sedimentary) - consists predominantly of sedimentary rock formations that are structurally weak, (b) less landslide-prone higher Himalayas (Central Crystalline) - comprising primarily of igneous and metamorphic rock with stronger and more stable formations, (c) barren land in the Trans-Himalayas (sedimentary) - characterized by cold desert and barren landscape, with sparse vegetation and exposed rock outcrops, (d) gully formation due to glacial erosion - glacial meltwater and the movement of glaciers have led to the formation of deep gullies and (e) dwarf deodar trees observed in Neylong Valley - features adaptation of vegetation, and (f) soil erosion due to snowmelt runoff - the snowmelt is prevalent, the runoff from melting snow causes erosion, particularly on slopes. This process removes the topsoil and can lead to the exposure of underlying rock.

4.2.3 | Field-based characterization of soil erosion processes and features

Field observations across the catchment revealed a diverse range of soil erosion processes controlled by lithology, elevation, vegetation cover, and hydrological dynamics. Among these, landslides constitute a dominant mechanism of soil redistribution, particularly along the stretch from Chamba to Bhatwari along NH-34 (Fig. 6a). While the frequency of landslides decreases towards Gangotri due to the presence of more resistant igneous and metamorphic rocks of the Central Crystalline zone (Fig. 6b), a critical anthropogenic driver of slope instability is unscientific road construction. In the Himalayan terrain, road expansion is often carried out through aggressive slope cutting, inadequate drainage planning, and improper disposal of excavated materials (muck), which significantly destabilize slopes. These practices weaken the natural structural integrity of hillslopes, making them highly susceptible to failure during the monsoon. As a result, road corridors act as hotspots of recurrent landslides, triggering large-scale soil loss and sediment transport every year. The repeated occurrence of such failures not only accelerates land degradation but also disrupts ecological stability and increases downstream sedimentation, highlighting the urgent need for slope-sensitive and scientifically designed infrastructure development in the Himalayas (Kaushal *et al*., 2025; Saha, and Bera, 2025). In the upper reaches, particularly from Bhaironghati near Harsil to the Neylong Valley and Pulam Sumda region, soils are generally shallow, immature, and loosely structured. These conditions, combined with sparse or absent vegetation, make the terrain highly susceptible to erosion. A clear altitudinal gradient in vegetation is observed, transitioning from dense forests to shrubs, grasses, and ultimately barren landscapes at higher elevations. In these Trans-Himalayan regions, erosion processes are further influenced by snowmelt, glacier dynamics, and gravity-driven mass movement (Fig. 6c-e). Continuous snowmelt contributes to the downslope transport of loose materials, often leaving behind exposed bedrock with minimal soil cover just below snow-capped zones (Fig. 6f).

Splash erosion was rarely observed, whereas sheet and rill erosion were more evident during or immediately after rainfall events. Residual signatures of sheet erosion were identified in the form of surface armouring, characterized by the depletion of fine particles and the relative enrichment of coarse fragments (Fig. 7a), resulting from the selective removal of silt and clay fractions (Wang and Shi, 2015). Vegetation cover plays a critical role in modulating erosion processes. Forested areas exhibited significantly lower surface runoff and soil loss due to the presence of leaf litter and multi-storey vegetation structure (Fig. 7b). The litter layer acts as a protective barrier, reducing raindrop impact and enhancing infiltration, while the underlying organic-rich horizon improves soil aggregation, porosity, and water retention (Zuazo and Pleguezuelo, 2009). Tree roots further stabilize the soil and limit downslope transport. Consequently, such areas generally lack well-defined concentrated flow features like gullies and are characterized by dark, organic-rich, and structurally stable soils. These conditions were predominantly observed on northern aspects of the catchment. However, localized erosion features were also identified within forested regions. Concentrated through-fall and channelized surface runoff can generate small gullies (Fig. 7c) and expose tree roots due to progressive soil removal (Fig. 7d), particularly where protective ground cover is disturbed (Vanwalleghem *et al*., 2003; Wallace *et al*., 2018).

In cultivated landscapes, terraces play a key role in modifying natural slope hydrology. While they generally reduce slope length and runoff velocity, improper maintenance and abandonment can lead to structural failure. Broken and collapsing terraces were observed in several locations (Fig. 7e), often resulting from excessive runoff from upslope areas and inadequate reinforcement (Tarolli *et al*., 2014). In addition, high overland flow in sloping agricultural fields was observed to bend grasses downslope, indicating flow direction and intensity, although such vegetation still provides partial protection against soil erosion (Fig. 7f). Overall, these field-based observations highlight the complex interactions between geomorphic processes, vegetation dynamics, and land-use practices in shaping soil erosion patterns across the Himalayan landscape.

4.2.4 | Soil erosion processes in alpine grasslands

In the alpine grasslands of the Himalayas, dense grass cover plays a vital role in protecting the soil surface by intercepting rainfall and minimizing the direct impact of raindrops (Marques *et al*., 2010). This vegetation layer reduces detachment of soil particles, enhances surface roughness, and promotes infiltration, thereby contributing to overall soil stability. However, these fragile ecosystems are highly sensitive to anthropogenic disturbances, particularly livestock grazing. Continuous trampling by livestock compacts the surface soil, leading to a decline in permeability and infiltration capacity (Fig. 8a). The compaction of moist, fine-textured soils especially those with higher silt content alters soil physical properties, resulting in the formation of a dense surface layer (Valentin, 1985). This hardened layer restricts water infiltration and increases both the volume and velocity of surface runoff (Dunne *et al*., 2011). Consequently, a larger proportion of rainfall is converted into overland flow, enhancing the detachment and transport of soil particles.

In addition to compaction, grazing activities disturb the protective grass cover. Hoof action dislodges and uproots vegetation, weakening the root network that binds the soil. The resulting bare patches become highly susceptible to erosion, as runoff preferentially flows through these exposed areas, removing fine soil particles and expanding the degraded zones (Fig. 8b). Runoff generated from upslope areas tends to concentrate in natural depressions within the grasslands. In the absence of sufficient vegetation cover, these flow paths intensify and initiate channelized erosion, eventually leading to gully formation (Fig. 8c). The dominant silt loam soils in these regions are inherently prone to erosion due to their fine texture and relatively low structural cohesion. As a result, gullies may progressively deepen and widen, in some cases extending down to the underlying bedrock, often limestone (Fig. 8d). Overall, while intact grass cover serves as an effective natural barrier against soil erosion, disturbances caused by grazing and trampling disrupt this equilibrium, significantly accelerating erosion processes. These observations highlight that, alongside natural drivers such as rainfall, snowmelt, and gravity, anthropogenic pressures play a crucial role in shaping soil erosion dynamics in alpine grasslands.

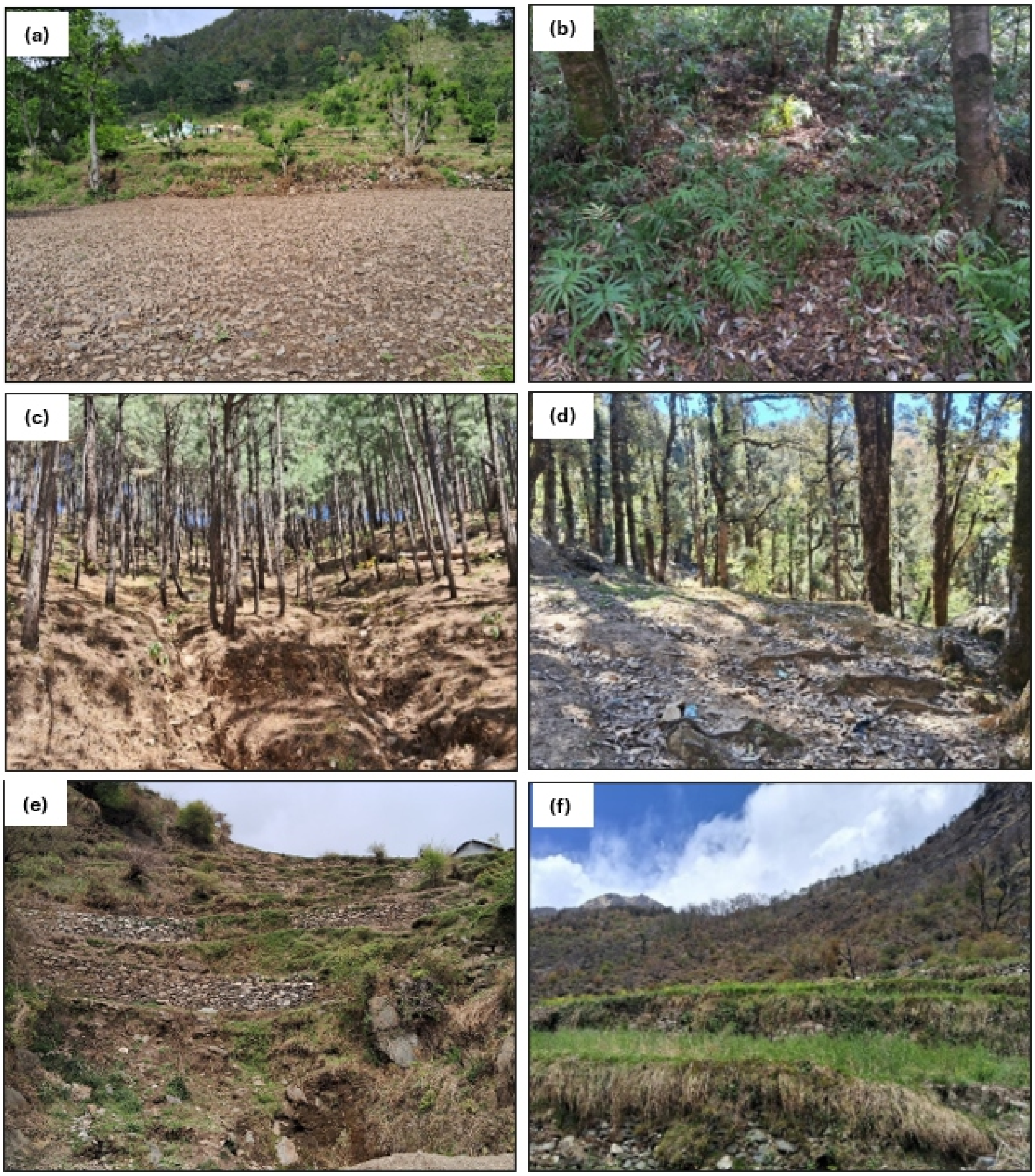

FIGURE 7 Soil erosion features observed in the Tehri dam catchment- (a) selective removal fine particle from cultivated land, (b) dense leaf litter cover observed in the forest- a thick layer of leaf litter covers the forest floor, providing a protective barrier against soil erosion, (c) gully erosion in the pine forest - where water has carved out deep channels in the soil, (d) exposed roots in the oak forest due to sheet erosion - leads to the gradual removal of the topsoil layer, (e) broken terraces in the field due to land abandonment - without proper maintenance, such as stone patching and vegetation management, the terraces fail to withstand the forces of erosion, and (f) slanted grasses observed at the edge of terraces safely dispose of overflow water.

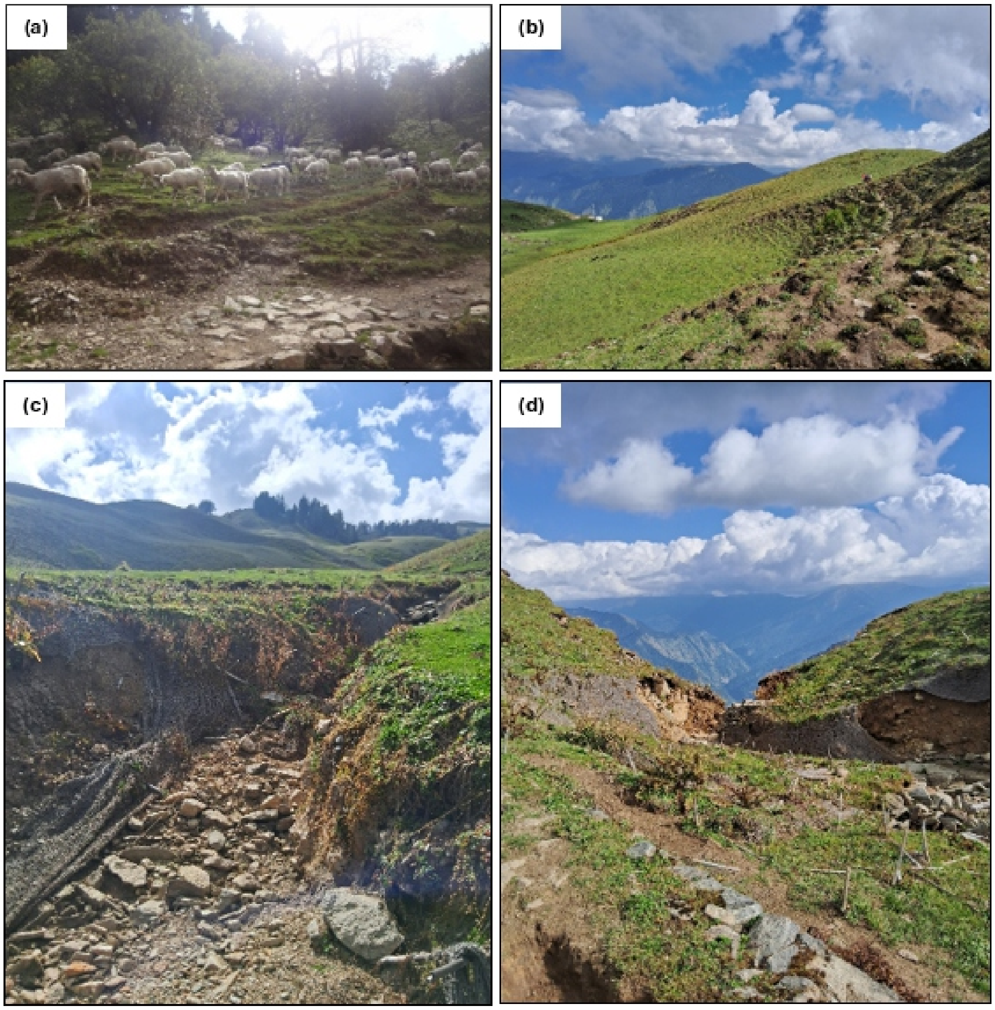

FIGURE 8 (a) Grazing by sheep - sheep feeding on grasses, impacting soil and vegetation, (b) soil removal due to trampling - soil erosion caused by the repetitive walking and trampling of sheep, (c) gully formation - deep channels created by water erosion, often exacerbated by the absence of vegetation, and (d) maximum vertical scouring of the gully up to bedrock - Severe erosion within the gully, eroding soil down to the underlying bedrock.

4.3 | Integration of field soil erosion indicators and ^{137}Cs-based soil erosion rates

Field-observed soil erosion indicators (Table 1), systematically documented during the survey (Section 4.2), were integrated with ^{137}Cs-derived soil erosion rates to establish a robust and field-applicable soil erosion classification framework for the Himalayan region. By linking qualitative visual indicators such as rills, gullies, pedestals, surface coarse fragments, and exposed roots with quantitative estimates of soil redistribution, a comprehensive approach was developed to assess erosion severity across diverse landscapes.

A detailed field campaign was conducted, combining visual assessment of erosion features with random-based soil sampling for ^{137}Cs analysis. At each sampling location, the dominant erosion processes and indicators were recorded and assigned to predefined erosion classes. These field-based classifications were then directly compared with the net soil erosion or deposition rates derived from the ^{137}Cs technique, enabling validation of the visual assessment approach. The accuracy of the visual soil erosion classification framework (E0-E6) was evaluated using confusion matrix-based metrics for both training and independent validation datasets. For the training dataset (n = 297), the classification framework achieved an overall accuracy (OA) of 76.8%, indicating that a substantial proportion of samples were correctly classified. The observed agreement (P_o) was 0.768, while the expected agreement (P_e) was 0.169. The resulting Kappa coefficient (κ) was 0.721, indicating substantial agreement between the visual classification and the ^{137}Cs-derived erosion rates. For the validation dataset (n = 74), the model demonstrated comparable performance, with an OA of 77.0%, P_o = 0.770, and P_e = 0.179, yielding a Kappa coefficient (κ) of 0.720. The close agreement between training and validation results

TABLE 1 Coding framework for rapid field assessment of soil erosion severity using visual indicators and ^{137}Cs-calibrated erosion rates in the Himalayas.

Code	Class	Erosion rate (t ha^{-1} yr^{-1})	Indicators
E0	No erosion	0	Characterized by a flat surface with fully covered soil, typically found in grass-covered flatlands. There are no surface coarse fragments or exposed roots, and the soil shows no signs of physical degradation such as compaction or crusting. The presence of an organic horizon and uniform soil colour further indicate a well-preserved soil structure and the absence of erosion.
E1	Very slight	0-5	Observed in soils with minimal disturbance and is characterized by the presence of an organic horizon. The soils are covered with litter and have a vegetation cover of 60-90%. Surface coarse fragments were minimal, ranging from 0-10%, with no exposed rock. The soil colour remains comparatively uniform. This condition is typically found in dense broad-leaved forests.
E2	Slight	5-10	Characterized by the trace of an organic horizon and the development of rills and small ephemeral gullies. The vegetation cover ranges from 50-70%, typically found on steep sloping terrain. Surface coarse fragments constitute 10-20%, and rocks are present. The soil colour is non-uniform with markings of water flow, and grasses or understory vegetation are often slanted towards the slope, indicating noticeable erosion processes. This is usually found in needle leaved moderately dense forest.
E3	Moderate	10-15	Absence of an organic horizon and the presence of high sheet and rill erosion, along with a high concentration of ephemeral gullies. Vegetation cover typically ranges from 30-50%, and surface coarse fragments constitute 20-25%. The soil colour is non-uniform, and there is an absence of understory growth. Slightly exposed rock and visible tree roots further indicate moderate erosion processes. This is usually found in scrub land/degraded forest.
E4	Moderately severe	15-20	This category is characterised by a high presence of surface coarse fragments exceeding 25%, and a vegetation cover of 20-50%, usually consisting of crops. The regions typically have terraces on steep slopes, with visible wash marks of soil erosion and signs of concentrated flow from subsequent terraces. Soil crusting is also evident, indicating significant soil degradation.
E5	Severe	20-40	This category is characterized by the presence of high surface coarse fragments exceeding 25%, with a vegetation cover ranging from 20-40%, often consisting of crops. The regions typically feature narrow terraces on steep or outward-sloping, with visible wash marks of soil erosion and broken or damaged terraces. The soil is light in colour, indicating severe soil degradation.
E6	Very severe	>40	Characterized by loose soils with minimal or no cover, often found on steep slopes. The soil depth is low, and there are severely exposed rocks. The soil is very light in colour, indicating extreme degradation, and an extensive network of large gullies is present, signifying severe erosion processes. Usually found in barren land.

indicates that the classification framework is robust and does not exhibit overfitting.

Class-wise accuracy metrics revealed clear variations in classification performance across erosion severity classes (Fig. 9). The producer's accuracy (PA) values ranged from 65.7% to 86.4% in the training dataset. The highest PA values were observed for E1 (86.4%), E0 (85.3%), and E6 (85.2%), indicating that very low and very high erosion conditions were reliably identified. In contrast, intermediate classes such as E2 (69.2%), E4 (68.2%), and E5 (65.7%) exhibited comparatively lower PA values, while E3 showed the highest PA (77.1%) relative to adjacent classes, reflecting increased classification uncertainty within transitional erosion zones. Similarly, the user's accuracy (UA) ranged from 55.6% to 100%. Higher UA values were recorded for E6 (100%), E5 (85.2%), E2 (83.1%), and E0 (82.9%), indicating strong reliability of predictions in these classes. In contrast, relatively lower UA values were observed for E4 (55.6%) and E3 (58.7%), suggesting a higher degree of commission error in these intermediate categories. Similar patterns, although differing in magnitude, were observed for the validation dataset (Fig. 9). These results indicate that misclassification predominantly occurred among adjacent erosion classes, particularly within the E2-E3 and E3-E4 transitions, where field indicators tend to overlap due to gradual changes in erosion intensity. The comparatively higher accuracy in extreme classes (E0 and E6) reflects the distinctiveness of visual indicators under very low and very high erosion conditions, whereas intermediate classes represent more complex and heterogeneous field conditions. Overall, the class-wise accuracy analysis demonstrates that while the classification framework performs strongly across most classes, the moderate uncertainty in transitional classes is consistent with the inherent continuum of soil erosion processes, rather than a limitation of the method itself. The Kappa coefficient obtained for both training and validation datasets indicates substantial agreement beyond chance, confirming the reliability of the visual classification framework. The relatively low expected agreement values (P_e = 0.169-0.179) further demonstrate that the observed agreement is not driven by random chance but reflects meaningful correspondence between field observations and quantitative erosion estimates. The observed Kappa of 0.72 for our framework indicates substantial agreement and compares favourably with previous visual appraisal studies. For instance, Okoba and Sterk (2006a) visual appraisals report model accuracy of 0.54-0.59, while remote sensing and modelling studies show wider ranges, including 51-82% overall accuracy for hyperspectral-based soil degradation mapping in the Czech Republic (Žížala *et al.,* 2017) and 0.28-0.66 model R^2 for aerial photography and erosion model-based mapping in the Danube Lowland, Slovakia (Jenčo *et al.*, 2020). These comparisons provide quantitative context for the reliability of the proposed visual indicator framework in mountainous Himalayan terrain. The consistency of accuracy metrics across independent datasets highlights the stability and generalizability of the classification system. The absence of significant deviation between training and validation performance suggests that the framework is robust and suitable for application across similar environmental conditions.

The results demonstrate that field-based visual indicators can effectively represent soil erosion severity when validated against quantitative methods such as ^{137}Cs analysis. Despite minor classification uncertainties in intermediate classes, the overall performance of the framework supports its use as a reliable and cost-effective tool for rapid field assessment. The strong agreement between visual indicators and radionuclide-derived erosion estimates underscores the potential of this approach for large-scale applications, particularly in data-scarce or resource-limited regions where detailed quantitative measurements may not be feasible.

The field-based soil erosion appraisal system developed for the north-western Himalayas (Table 1) provides a systematic framework for classifying erosion severity by integrating observable surface indicators with corresponding quantitative erosion rates. The classification ranges from E0 (no erosion) to E6 (very severe erosion), covering a gradient of soil loss from stable, well-protected surfaces to highly degraded, erosion-prone landscapes. Each class is defined based on a combination of key field

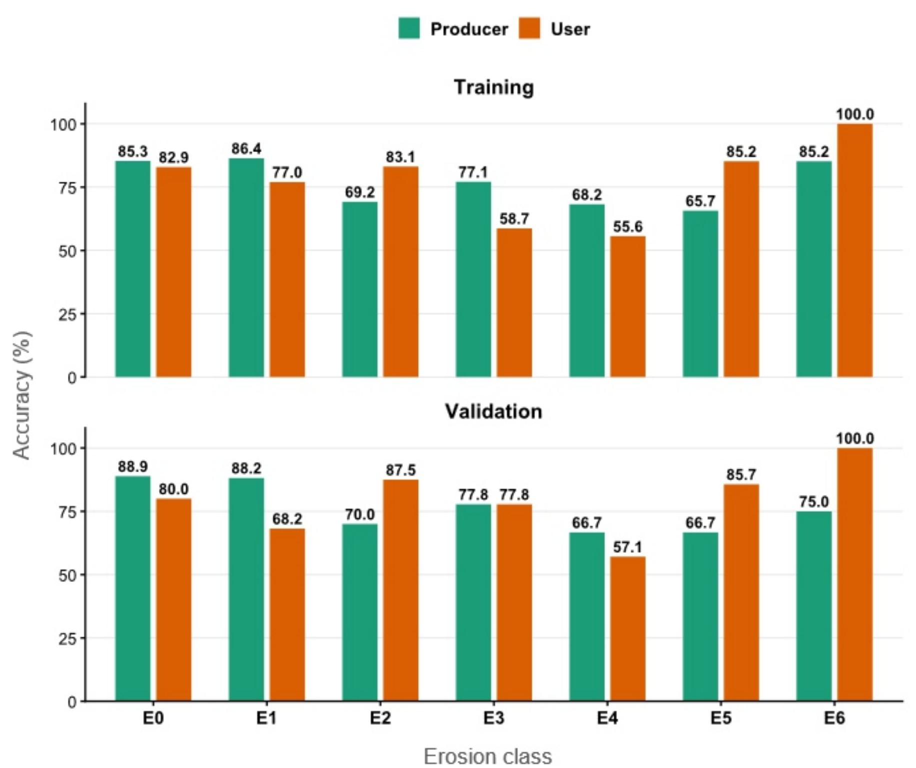

FIGURE 9 Distribution of Producer's and User's accuracy of various erosion classes.

indicators, including vegetation cover, presence or absence of an organic horizon, surface coarse fragments, soil colour variation, and visible erosion features such as rills, gullies, exposed roots, and terrace degradation. Lower classes (E0-E1) represent stable environments with dense vegetation cover, intact soil structure, and minimal disturbance, typically observed in grasslands and dense forests. Intermediate classes (E2-E4) reflect increasing erosion intensity, marked by the development of rills, ephemeral gullies, reduction in vegetation cover, and evidence of surface runoff and soil crusting, often associated with degraded forests and cultivated slopes. Higher classes (E5-E6) indicate severe to very severe erosion conditions, characterized by sparse or absent vegetation, high coarse fragment concentration, exposed bedrock, broken terraces, and well-developed gully networks, commonly found in agricultural and barren landscapes. This coding system enables rapid field-based assessment of soil erosion severity and serves as a critical link between qualitative visual indicators and quantitative ^{137}Cs-derived soil erosion rates, thereby enhancing the reliability and applicability of erosion mapping in complex Himalayan terrains.

To support the interpretation of erosion severity classes and enhance the practical applicability of the proposed framework, representative field photographs corresponding to each erosion class (E0-E6) are presented (Fig. 10). These images illustrate the characteristic field conditions associated with different levels of erosion, including variations in vegetation cover, soil surface condition, presence of coarse fragments, and development of erosion features such as rills, gullies, pedestals, and morphology. The progression from stable, well-covered surfaces in lower classes (E0-E1) to highly degraded, sparsely vegetated, and structurally unstable conditions in higher classes (E5-E6) is clearly evident. These visual references not only substantiate the classification scheme derived from field observations and ^{137}Cs-based erosion rates but also provide a practical basis for comparing and validating erosion severity across different sites. The inclusion of such field evidence strengthens the reliability of the classification framework and facilitates its use in future studies and field-based erosion assessments in similar mountainous environments.

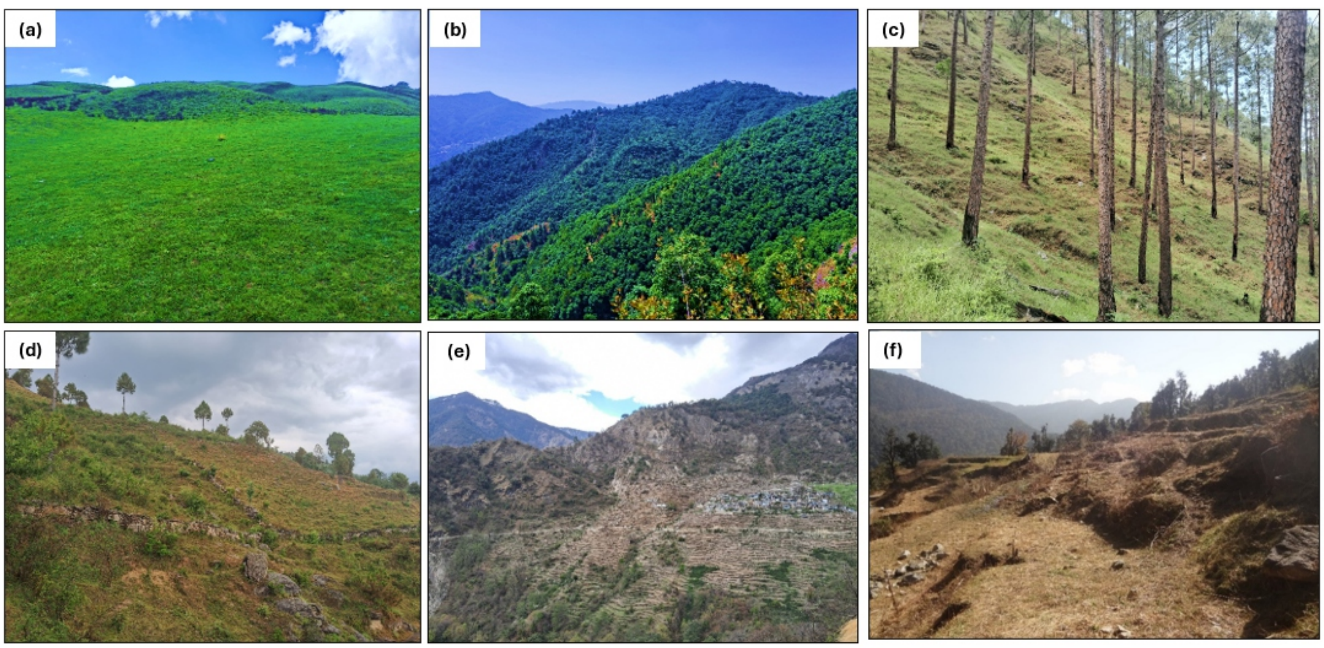

FIGURE 10 Representative field conditions illustrating soil erosion severity classes (E0-E6) in the Himalayan region- (a) E0 - No erosion: Flat grassland with dense, continuous vegetation cover and dark, organic-rich soil, indicating stable surface conditions and absence of erosion, (b) E1 - Very slight erosion: Dense broadleaved forest with high litter accumulation and minimal disturbance, reflecting well-protected soil and negligible erosion, (c) E2 - Slight erosion: Pine-dominated forest with limited or no understory vegetation, showing early signs of surface disturbance and minor erosion features, (d) E3 - Moderate erosion: Scrubland with sparse trees and bushes, reduced vegetation cover, and visible surface degradation indicating active erosion processes, (e) E4 - Moderately severe erosion: Steep, terraced agricultural land with evident soil movement, wash marks, and partial instability of terraces, and (f) E5 - Severe erosion: steep slopes, exposed rocks, and light-coloured soil and broken terraces. (For E6 please refer Figure 6 c.)

4.4 | Soil quality variations across erosion classes

The spatial variability of soil physico-chemical properties across land use/land cover (LULC) types provides contextual evidence supporting the patterns observed in the erosion severity classes derived from visual indicators and Caesium-137 tracing. A clear and consistent trend emerges in which soil quality declines with increasing erosion intensity, reflecting the progressive loss of fertile topsoil and structural degradation. Sites classified under low erosion classes (E0-E2), predominantly associated with forest and grassland ecosystems, exhibited comparatively better soil health, characterized by higher soil organic carbon (SOC), lower bulk density (BD), stable soil structure, and relatively balanced texture with higher retention of fine particles. These conditions indicate minimal disturbance and effective protection against erosive forces due to dense vegetation cover and organic matter inputs. In contrast, moderate to high erosion classes (E3-E6), largely corresponding to scrubland, agricultural, and barren land, showed clear signs of soil degradation, including reduced SOC, increased BD, coarser texture due to selective removal of silt and clay fractions, and greater variability in soil pH and electrical conductivity. The elevated bulk density and reduced organic matter in these areas indicate compaction and diminished soil aggregation, which further enhance susceptibility to erosion. Agricultural lands, particularly under intensive cultivation, exhibited intermediate characteristics, where practices such as tillage and terrace farming influenced soil redistribution, often leading to localized accumulation of finer particles but overall decline in soil quality. Similarly, scrubland and barren areas, associated with higher erosion classes, displayed depleted nutrient status and poor structural stability due to limited vegetation cover and continuous soil loss. The observed correspondence between soil properties, land use/land cover, and erosion classes reinforces the reliability of both the visual indicator-based classification and the ^{137}Cs-derived erosion rates. Studies across diverse regions indicate that soil quality indices, productivity indices, and microbial activity decrease as erosion intensity increases (Fang *et al*., 2024; Mandal *et al.*, 2021 and 2023). This integrated relationship demonstrates that erosion not only redistributes soil but also systematically alters its physico-chemical properties, thereby providing a robust basis for validating erosion assessment approaches in complex mountainous environments.

4.5 | Limitation of the study

All field observations were conducted by a single observer to ensure consistency in the identification and classification of visual soil erosion indicators. To minimize subjectivity and improve reproducibility, a standardized field observation questionnaire was used to assign erosion classes based on predefined criteria. Although this approach ensured internal consistency, inter-observer variability was not evaluated. Future studies should involve multiple observers to assess the reproducibility and transferability of the proposed framework across different users and environmental settings.

Another limitation relates to the difference in the temporal scales represented by the two assessment methods. The ^{137}Cs-derived soil redistribution rates integrate erosion and deposition processes over approximately the past six decades, whereas visual soil erosion indicators primarily reflect persistent or repeatedly occurring erosion features rather than erosion occurring at a single point in time. For example, gullies and pedestals develop over relatively long periods, while sheet and rill erosion may be seasonal, and vegetation-related indicators often represent the cumulative effects of soil loss over multiple years. Consequently, the two approaches provide complementary rather than identical information: ^{137}Cs measurements quantify long-term average soil redistribution, whereas visual indicators characterize the spatial expression and relative severity of persistent erosion processes.

Future research should evaluate the applicability of the framework across different climatic regions, soil types, and land-use systems, and incorporate multiple observers to quantify observer-related uncertainty. In addition, the integration of short-term fallout radionuclides, such as excess ^{210}Pb ($^{210}Pb_{ex}$) and beryllium-7 (^{7}Be), could enable assessment of more recent soil redistribution, thereby improving the temporal correspondence between radionuclide-derived erosion rates and visual field indicators.

5 | CONCLUSIONS

The study developed and validated a practical framework for rapid soil erosion assessment in the Himalayan region by integrating visual soil erosion indicators with quantitative ^{137}Cs-derived soil erosion rates. The results demonstrate that readily observable field indicators can be reliably linked to measured soil erosion magnitudes, enabling the development of a calibrated visual indicator–erosion rate framework. The substantial agreement between visually interpreted erosion classes and radionuclide-derived erosion rates (Cohen's Kappa = 0.72) confirms the robustness and reliability of the proposed approach. The study further demonstrates that erosion severity is strongly associated with land use and soil quality. Forest and grassland ecosystems, corresponding to lower erosion classes, exhibited higher soil organic carbon, lower bulk density, and better soil structural stability. In contrast, scrubland, agricultural land, and barren areas were characterized by higher erosion rates, reduced organic matter, increased soil compaction, and coarser soil texture resulting from the preferential removal of fine particles. These findings highlight the close interactions among land use, soil degradation, and erosion processes in fragile Himalayan landscapes. A major outcome of this research is the development of a field-applicable E0-E6 visual erosion classification framework, supported by representative field photographs and standardized observation guidelines. Unlike conventional erosion assessment techniques that require extensive field measurements, laboratory analyses, or complex modelling, the proposed framework enables rapid, low-cost, and instrument-free estimation of soil erosion severity using only observable field indicators. The validated approach can be readily applied by researchers, land managers, extension personnel, and local practitioners without requiring radionuclide measurements or specialized equipment. Beyond its application for rapid field assessment, the framework provides an independent tool for validating soil erosion models, supporting large-scale erosion mapping, and generating reliable training datasets for machine-learning-based erosion prediction. Its simplicity and scalability make it particularly valuable for data-scarce and inaccessible mountainous regions where conventional monitoring approaches are often impractical. By bridging rigorous radionuclide-based measurements with field-level usability, this study provides an operational framework that enhances the accuracy, efficiency, and accessibility of soil erosion assessment. The approach offers significant potential for supporting evidence-based watershed management, soil conservation planning, and sustainable land management in the Himalayas and other erosion-prone mountain environments.

ACKNOWLEDGEMENTS

The study was supported by the Indian Space Research Organisation (ISRO) through financial assistance under the Earth Observation Applications Mission (EOAM) Project (ISRO/DOS) titled 'Mountain Ecosystem Processes and Services – Phase II: Soil Erosion Estimation based on Radio Tracer Technique and Soil Quality Assessment in the Mountainous Landscape of the North-West Himalaya'. We sincerely thank the Commanding Officer and personnel of the Jammu and Kashmir Light Infantry (Indian Army) for their support during soil sampling in the highly vulnerable terrain of Nelong Valley and surrounding areas. We are grateful to the District Administration for granting permission to conduct fieldwork in restricted regions. We also acknowledge the support of the Uttarakhand Forest Department and the authorities of Gangotri National Park for permitting and facilitating soil sample collection across Uttarkashi and Tehri Garhwal. We are also thankful to the Director, Indian Institute of Remote Sensing (IIRS) for providing the necessary facilities to carry out this research work.

CONFLICT OF INTEREST

The authors declare that they have no known competing financial interests or personal relationships that could have appeared to influence the work reported in this paper.

DATA AVAILABILITY STATEMENT

The data that support the findings of this study are available in the tables, figures and published sources.

AUTHOR'S CONTRIBUTION

Conceptualization and Methodology - Anu David Raj; Validation - Suresh Kumar, Sankar M..; Investigation - Anu David Raj; & K. R. Sooryamol; Resources - Suresh Kumar & Anu David Raj & K. R. Sooryamol; Writing - Original Draft - Anu David Raj & K.R. Sooryamol; Review & Editing - Suresh Kumar, Sankar M..; Visualization - Anu David Raj; Sample collection & Soil Analysis- K R. Sooryamol & Anu David Raj; Supervision - Suresh Kumar & Sankar M; Project administration - Suresh Kumar; Funding acquisition - Suresh Kumar

REFERENCES

Arata, L., Meusburger, K., Frenkel, E., A'Campo-Neuen, A., Iurian, A.R., Ketterer, M.E., Mabit, L. and Alewell, C. 2016. Modelling deposition and erosion rates with RadioNuclides (MODERN)–Part 1: A new conversion model to derive soil redistribution rates from inventories of fallout radionuclides. *J. Environ. Radioact*., 162: 45-55.

Batista, P., Davies, J., Silva, M. and Quinton, J. 2019. On the evaluation of soil erosion models: Are we doing enough? *Earth-Sci. Rev*. DOI: 10.1016/j.earscirev.2019.102898.

Beck, H.E., Zimmermann, N.E., McVicar, T.R., Vergopolan, N., Berg, A. and Wood, E.F. 2018. Present and future Köppen-Geiger climate classification maps at 1-km resolution. *Sci. Data,* 5(1): 1-12.

Borrelli, P., Alewell, C., Alvarez, P., Anache, J.A.A., Baartman, J., Ballabio, C., Bezak, N., Biddoccu, M., Cerdà, A., Chalise, D. and Chen, S. 2021. Soil erosion modelling: A global review and statistical analysis. *Sci. Total Environ*., 780: 146494.

Chauhan, D.S., Chauhan, R., Shankar, B. and Kesari, G.K. 2022. Structural and kinematic study of Ghuttu Window: Implication on the tectonic evolution of Bhilangana Formation, Central Crystalline Group, Garhwal Himalaya, India. *J. Earth Syst. Sci.,* 131(4): 197.

Chandrakala, M., Maske, S., Anil Kumar, K.S., Parvathy, S., Chakraborty, R., Karthika, K.S., Ramesh Kumar, S.C. and Ramamurthy, V. 2024. Soil erosion estimation and mapping using detailed soil survey and GIS: Need for soil conservation in hilly areas, tropical humid region, India. *Indian J. Soil Cons*., 52(3): 207-216. DOI: 10.59797/ijsc.v52.i3.174.

Clubb, F.J., Mudd, S.M., Attal, M., Milodowski, D.T. and Grieve, S.W. 2016. The relationship between drainage density, erosion rate, and hilltop curvature: Implications for sediment transport processes. *J. Geophys. Res. Earth Surf.*, 121(10): 1724-1745.

David Raj, A. and Kumar, S. 2024. Fallout radionuclide (^{137}Cs) method for quantifying soil erosion rates in steep sloping hilly and mountainous landscapes of Himalayas. In: Intelligence Systems for Earth, Environmental and Planetary Sciences, pp. 261-289. Elsevier.

David Raj, A., Kumar, S., and Sooryamol, K. R. 2022. Modelling climate change impact on soil loss and erosion vulnerability in a watershed of Shiwalik Himalayas. *Catena*, 214: 106279.

David Raj, A., Kumar, S., Kalambukattu, J. G. and Chatterjee, U. 2024a. Land degradation and its relation to climate change and sustainability. In Climate Crisis: *A*daptive Approaches and Sustainability (pp. 121–135). Cham: Springer Nature Switzerland.

David Raj, A., Kumar, S., Mariappan, S., Sooryamol, K. R., and Kalambukattu, J. G. 2024d. Potential of pine forest in controlling soil erosion in Himalayan region—Investigation using fallout radionuclide (^{137}Cs) measurements. *Evolving Earth*, 2: 100031.

David Raj, A., Kumar, S., Sooryamol, K. R., Kalambukattu, J. G., and Kumara, S. 2024b. Soil redistribution rates along the forested and cultivated steep hillslope in the mid-Himalayas using fallout—^{137}Cs and RUSLE model. *Land Degrad. Dev.*, 35(16): 4795–4813.

David Raj, A., Kumar, S., Sooryamol, K.R., Mariappan, S. and Kalambukattu, J.G. 2024c. ^{137}Cs radiotracer in investigating influence of hillslope positions and land use on soil erosion and soil organic carbon stock—A case study in the Himalayan region. *Soil Use Manag.,* 40(3): e13099.

David Raj, A., Kumar, S., Sooryamol, K.R., Sankar, M. and George, J.K. 2025a. Quantifying soil redistribution across Himalayan hillslope under the influence of topography and terrace abandonment using fallout-^{137}Cs. *Discover Geosci.*, 3(1): 233.

David Raj, A., Kumar, S., Sooryamol, K.R., Sankar, M. and George, K.J. 2025b. Assessment of soil erosion rates, carbon stocks, and erosion-induced carbon loss in dominant forest types of the Himalayan region using fallout-^{137}Cs. *Sci. Rep.*, 15(1): 14950.

David Raj, A., Kumar, S., Sankar, M. and Sooryamol, K.R. 2026. Soil erosion rates, driving factors and climate change impacts across different land uses in the Himalayas: Insights from Caesium-137

(^{137}Cs) tracing and the revised universal soil loss equation (RUSLE) model. Sci. *Total Environ*., 1048: 182034.

Del Pino, J.S.N. and Ruiz-Gallardo, J.R. 2015. Modelling post-fire soil erosion hazard using ordinal logistic regression: a case study in South-eastern Spain. *Geomorphology*, *232*: pp.117-124.

Dexter, A.R., Czyż, E.A., Birkás, M., Diaz-Pereira, E., Dumitru, E., Enache, R., Fleige, H., Horn, R., Rajkaj, K., De La Rosa, D. and Simota, C. 2005. SIDASS project: Part 3. The optimum and the range of water content for tillage–further developments. *Soil Tillage Res.*, *82*(1): pp.29-37.

Dorji, T., Odeh, I.O., Field, D.J. and Baillie, I.C. 2014. Digital soil mapping of soil organic carbon stocks under different land use and land cover types in montane ecosystems, Eastern Himalayas. *For. Ecol. Manage.*, 318: 91-102.

Dunne, T., Western, D. and Dietrich, W.E. 2011. Effects of cattle trampling on vegetation, infiltration, and erosion in a tropical rangeland. *J. Arid Environ.,* 75(1): 58-69.

Fang, H., Zhai, Y. and Li, C. 2024. Evaluating the impact of soil erosion on soil quality in an agricultural land, northeastern China. *Sci. Rep*., 14: 15629 DOI: 10.1038/s41598-024-65646-5.

Gupta, S. and Kumar, S. 2017. Simulating climate change impact on soil erosion using RUSLE model—A case study in a watershed of mid-Himalayan landscape. *J. Earth Syst. Sci.*, 126(3): p.43.

IAEA. 2014. Guidelines for using fallout radionuclides to assess erosion and effectiveness of soil conservation strategies. In: *IAEA-TECDOC 1741* (pp. 226). International Atomic Energy Agency, Vienna.

IMD, 2014. *Climate of Uttarakhand*. Additional Director General of Meteorology (Research), Climatological Summaries of States Series - No. 21, India Meteorological Department, Pune – 125 p.

Jain, S.K., Kumar, S. and Varghese, J. 2001. Estimation of soil erosion for a Himalayan watershed using GIS technique. *Water Resour. Manag.*, 15(1): 41-54.

Jaleta Negasa, D. 2020. Effects of land use types on selected soil properties in Central Highlands of Ethiopia, *Appl. Environ. Soil Sc*i., 2020: 7026929, DOI: 10.1155/ 2020/7026929.

Jenco, M., Fulajtár, E., Bobáľová, H., Matečný, I., Saksa, M., Kožuch, M., Gallay, M., Kaňuk, J., Píš, V. and Oršulová, V. 2020. Mapping soil degradation on arable land with aerial photography and erosion models, case study from Danube Lowland, Slovakia. *Remote Sens.,* 12(24): 4047.

Joshi, P., Adhikari, R., Bhandari, R., Shrestha, B., Shrestha, N., Chhetri, S., Sharma, S. and Routh, J. 2023. Himalayan watersheds in Nepal record high soil erosion rates estimated using the RUSLE model and experimental erosion plots. *Heliyon*, *9*(5).

Kalambukattu, J.G., Suresh Kumar, S. and Hole, R.M. 2021. Geospatial modelling of soil erosion and risk assessment in Indian Himalayan region—A study of Uttarakhand state. *Environ. Adv.*, 4: 100039.

Karunakara, N., Chetan,R., Ujwal, P., Yashodhara, I., Sudeep Kumara,K., Ravi, P.M. 2013.Soil to rice transfer factors for ^{226}Ra, ^{228}Ra, ^{210}Pb, ^{40}K and ^{137}Cs: a study on rice grown in India. *J. Environ. Radioact.*, 118: 80–92.

Kaushal, S., Thanveer, J., ul Islam, S.M., Negi, A., Dhanshyan, A., Beetan, Y., Subramanian, S.S., Sajinkumar, K.S. and Yunus, A.P. 2025. Unveiling the amplifying impact: Anthropogenic activities and the two-fold surge in landslides in the Lesser Himalayas. *Catena*, *250*: p.108771.

Keller, T. and Håkansson, I. 2010. Estimation of reference bulk density from soil particle size distribution and soil organic matter content. *Geoderma*, *154*(3-4): pp.398-406.

Koiter, A.J., Owens, P.N., Petticrew, E.L. and Lobb, D.A. 2017. The role of soil surface properties on the particle size and carbon selectivity of interrill erosion in agricultural landscapes. *Catena*, *153*: pp.194-206.

Kumar, S., David Raj, A., and Mariappan, S. 2024a. Fallout radionuclides (FRNs) for measuring soil erosion in the Himalayan region: A versatile and potent method for steep sloping hilly and mountainous landscapes. *Catena*, *234*: p.107591.

Kumar, S., David Raj, A., Mariappan, S., Kalambukattu, J.G., Sooryamol, K.R., Singh, R.P., Madhu, M. and Karunakara, N. 2024b. Application of fallout radionuclide—137Cs for estimating soil erosion in steep hillslopes with diverse land use of North-western Indian Himalayas. *Discover Environ., 2*(1): 105.

Kumar, S., Murugan, N., David Raj, A. and George Kalambukattu, J. 2023. Hillslope elements and soil–landscape analysis in Himalayas for characterizing soil quality parameters using digital terrain model and remote-sensing data. *Environ. Earth Sci.*, *82*(20): 469.

KVK, n.d. Tehri Garhwal, District Profile, Available at https://tehrigarhwal.kvk4.in/district-profile.html, Accessed on 25 June 2024.

Legout, C., Leguédois, S. and Le Bissonnais, Y. 2005. Aggregate breakdown dynamics under rainfall compared with aggregate stability measurements. *Eur. J. Soil Sci., 56*(2): 225-238.

Loughran, R.J., Wallbrink, P.J., Walling, D.E. and Appleby, P.G. 2002. Sampling Methods. In: Zapata, F. (eds.) *Handbook for the Assessment of Soil Erosion and Sedimentation Using Environmental Radionuclides*. Springer, Dordrecht. https://doi.org/10.1007/0-306-48054-9_3.

Mabit, L., Bernard, C., Lee Zhi Yi, A., Fulajtar, E., Dercon, G., Zaman, M. and Heng, L. 2018. Promoting the use of isotopic techniques to combat soil erosion: An overview of the key role played by the SWMCN Subprogramme of the Joint FAO/IAEA Division over the last 20 years. *Land Degrad. Dev*., 29(9): 3077-3091.

Mandal, D., Chandrakala, M., Alam, N., Roy, T. and Mandal, U. 2021. Assessment of soil quality and productivity in different phases of soil erosion with the focus on land degradation neutrality in tropical humid region of India. *Catena*, 204: 105440. DOI: 10.1016/j.catena.2021.105440.

Mandal, D., Patra, S., Sharma, N., Alam, N., Jana, C. and Lal, R. 2023. Impacts of Soil Erosion on Soil Quality and Agricultural Sustainability in the North-Western Himalayan Region of India. *Sustainability*. DOI: 10.3390/su15065430.

Mariappan, S., Hartley, I.P., Cressey, E.L., Dungait, J.A. and Quine, T.A. 2022. Soil burial reduces decomposition and offsets erosion-induced soil carbon losses in the Indian Himalaya. *Glob. Change Biol.*, 28(4): 1643-1658.

Marques, M.J., García-Muñoz, S., Muñoz-Organero, G. and Bienes, R. 2010. Soil conservation beneath grass cover in hillside vineyards under Mediterranean climatic conditions (Madrid, Spain). *Land Degrad. Dev.,* 21(2): 122-131.

Mekonnen, M., Keesstra, S.D., Stroosnijder, L., Baartman, J.E. and Maroulis, J. 2015. Soil conservation through sediment trapping: A review. *Land Degrad. Dev*., 26(6): 544-556.

Meusburger, K., Mabit, L., Park, J.H., Sandor, T. and Alewell, C. 2013. Combined use of stable isotopes and fallout radionuclides as soil erosion indicators in a forested mountain site, South Korea. *Biogeosciences*, *10*(8): 5627-5638.

Mohan, M.P., D'Souza, R.S., Nayak, S.R., Kamath, S.S., Shetty, T., Kumara, K.S., Mayya, Y.S. and Karunakara, N. 2019. Influence of rainfall on atmospheric deposition fluxes of ^{7}Be and ^{210}Pb in Mangaluru (Mangalore) at the Southwest Coast of India. *Atmos. Environ.,* 202: 281-295.

Müller, T.S., Dechow, R. and Flessa, H. 2022. Inventory and assessment of pH in cropland and grassland soils in Germany. J. *Plant Nutr. Soil Sci*., 185(1): 145-158.

Nadelhoffer, K. J. Boone, R.D., Bowden, R. D., Canary, J. D., Kaye, J., Micks, P., Ricca, A., Aitkenhead, J. A., Lajtha, K. and McDowell, W.H. 2004. The DIRT experiment: litter and root influences on forest soil organic matter stocks and function. Chapter 15 in: D. Foster and J. Aber (eds.), *Forest Landscape Dynamics in New England: Ecosystem Structure and Function as a Consequence of 5000 years of Change*. Synthesis Volume of the Harvard Forest LTER Program Oxford University Press.

Okoba, B. and Sterk, G. 2006a. Quantification of visual soil erosion indicators in Gikuuri catchment in the central highlands of Kenya. *Geoderma*, 134: 34-47. https://doi.org/10.1016/j.geoderma.2005.08.013.

Okoba, B. and Sterk, G. 2006b. Farmers' identification of erosion indicators and related erosion damage in the Central Highlands of Kenya. *Catena*, 65: 292-301. https://doi.org/10.1016/j.catena.2005.12.004.

Óskarsson, H., Arnalds, Ó., Gudmundsson, J. and Gudbergsson, G. 2004. Organic carbon in Icelandic Andosols: geographical variation and impact of erosion. *Catena*, 56(1-3): 225-238.

Padarian, J., Stockmann, U., Minasny, B. and McBratney, A.B. 2022. Monitoring changes in global soil organic carbon stocks from space. *Remote Sens. Environ*., 281: 113260.

Pai, D.S., Rajeevan, M., Sreejith, O.P., Mukhopadhyay, B., and Satbha, N. S. 2014. Development of a new high spatial resolution (0.25× 0.25) long period (1901-2010) daily gridded rainfall data set over India and its comparison with existing data sets over the region. *Mausam*, 65(1): 1-18.

Raj, A.D. 2025. *Geospatial modelling in soil erosion estimation using radioisotope tracer technique and climate change impact assessment in the north-western Himalayan region*. PhD thesis, Forest Research Institute, Dehradun, 315 p.

Saha, S. and Bera, B. 2025. Char Dham highway construction and the surge in landslide frequency and magnitude in the Garhwal Himalayas, India. *Geotech. Geol. Eng.*, 43(6): 266.

Salhi, A., El Hasnaoui, Y., Pérez Cutillas, P. and Heggy, E. 2023. Soil erosion and hydroclimatic hazards in major African port cities: The case study of Tangier. *Sci. Rep.*, 13(1): 13158.

Sarmiento, L., Bottner, P., 2002. Carbon and nitrogen dynamics in two soils with different fallow times in the high tropical Andes: indications for fertility restoration. *Appl. Soil Ecol.* 19: 79–89. http://dx.doi.org/10.1016/S0929-1393(01)00178-0.

Sidhu, G.S. and Surya, J.N. 2014. Soils of North-Western Himalayan eco-system and their land use, constraints, productivity potentials and future strategies. *Agropedology*, 24 (01): 1-19.

Singh, S.K., Singh, A.K., Sharma, B.K. and Tarafdar, J.C. 2007. Carbon stock and organic carbon dynamics in soils of Rajasthan, India. *J. Arid Environ.*, 68(3): 408-421.

Singh, A.K., Kumar, S., Naithani, S., K, George, J. 2019. Soil erosion and sediment yield estimation using remote sensing data and GIS in a Sitlarao watershed of north-western Himalayan region. *Indian J. Soil Cons., 47(3): 244-254.*

Sooryamol, K.R., Kumar, S., Regina, M., and David Raj, A. 2022. Modelling climate change impact on soil erosion in a watershed of north-western lesser Himalayan region. *J. Sediment. Environ*., 7(2): 125-146.

Tarolli, P., Preti, F. and Romano, N. 2014. Terraced landscapes: From an old best practice to a potential hazard for soil degradation due to land abandonment. *Anthropocene*, *6*: 10-25.

Uppengal, S., Raj, A. D., Padmavathi, B., Nameer, P. O., and Nair, J. G. 2026. Soil erosion responses to climate change in a tropical monsoon-dominated river basin - A geospatial perspective. *River,* 5(2): 222-249. https://doi.org/10.1002/rvr2.70054.

Valentin, C. 1985. Effects of grazing and trampling on soil deterioration around recently drilled water holes in the Sahelian zone. In: El Swaify S.A. (ed.), Moldenhauer W.C. and Lo, A. (eds.). Soil erosion and conservation. Ankeny, Iowa : Soil Conservation Society of America, pp. 51-65. International Conference on Soil Erosion and Conservation, Honolulu (USA), 16-22 January 1983.

Vanwalleghem, T., Van Den Eeckhaut, M., Poesen, J., Deckers, J., Nachtergaele, J., Van Oost, K. and Slenters, C. 2003. Characteristics and controlling factors of old gullies under forest in a temperate humid climate: a case study from the Meerdaal Forest (Central Belgium). *Geomorphology*, 56(1-2): 15-29.

Wallace, C.W., McCarty, G., Lee, S., Brooks, R.P., Veith, T.L., Kleinman, P.J. and Sadeghi, A.M., 2018. Evaluating concentrated flowpaths in riparian forest buffer contributing areas using LiDAR imagery and topographic metrics. *Remote Sens.*, *10*(4): 614.

Wang, L. and Shi, Z.H. 2015. Size selectivity of eroded sediment associated with soil texture on steep slopes. *Soil Sci. Soc. Am. J., 79*(3): 917-929.

Yang, S., Cammeraat, E., Jansen, B., De Haan, M., Van Loon, E.E. and Recharte, J. 2018. Soil organic carbon stocks controlled by lithology and soil depth in a Peruvian alpine grassland of the Andes. *Catena,* 171: 22–31. https://doi.org/10.1016/j.catena.2018.06.038.

Žížala, D., Zádorová, T. and Kapička, J. 2017. Assessment of soil degradation by erosion based on analysis of soil properties using aerial hyperspectral images and ancillary data, Czech Republic. *Remote Sens*., 9(1): 28.

Zuazo, V.H.D., Pleguezuelo, C.R.R. 2009. Soil-Erosion and Runoff Prevention by Plant Covers: A Review. In: Lichtfouse, E., Navarrete, M., Debaeke, P., Véronique, S., Alberola, C. (eds.) *Sustainable Agriculture*. Springer, Dordrecht. https://doi.org/10.1007/978-90-481-2666-8_48.

How to cite this article: David Raj, A., Sooryamol, K. R., Kumar, S. and Sankar, M., 2026. Linking Visual Soil Erosion Indicators with FRN-^{137}Cs-Derived Soil Erosion Rates for Rapid Field-Based Soil Erosion Assessment in the Himalayan Region *Indian J. Soil Cons*., 54(2): 99-118.